DYNAMICAL FORMULATION OF TRANSITION STATE THEORY: VARIATIONAL TRANSITION STATES AND SEMICLASSICAL TUNNELING

Susan C. Tucker and Donald G. Truhlar
Department of Chemistry and Supercomputer Institute
University of Minnesota
Minneapolis, MN 55455, U.S.A.

ABSTRACT. This paper is an introduction to recent research in generalized transition state theory. We derive the theory by considering the equilibrium flux through a surface dividing reactants from products, and we show its equivalence to the quasi–thermodynamic formulation of transition state theory. We show that conventional transition state theory is obtained from the generalized theory with a specific choice of dividing surface, but we stress that in many cases the variational identification of the transition state provides significant improvement. We discuss methods for including quantum effects, with special attention to the semiclassical treatment of tunneling. We briefly review tests of the theory and applications to gas–phase, condensed–phase, and interface reactions. Finally we discuss the importance of nonsubstantial contributions to quasi–thermodynamic quantities.

1. Introduction

Transition state theory (TST) has been the most widely used framework for the interpretation of reaction rate constants for many years [1,2]. Transition state theory is used in two quite different ways, which we will call the phenomenological approach and the absolute rate theory approach. In the former, experimental data are interpreted using transition state theory concepts, and — in favorable cases — parameters characterizing the transition state or the barrier to tunneling are extracted. In the latter, rate constants are calculated using semiempirical or *ab initio* information either about the electronic forces on the nuclei or about the Born–Oppenheimer potential energy hypersurface (which is usually just called the "energy surface"). Recent research on the latter approach, including both variational generalizations of the conventional theory and improved methods for calculating tunneling contributions, has led to much better estimates of the accuracy that can be achieved with this method than were previously available. It has also led to a better understanding of dynamical bottlenecks and tunneling paths, allowing us to interpret the phenomenological parameters obtained from experiment, even in cases where full force fields or energy surfaces are unavailable, and, consequently, full rate constant calculations cannot be performed. In the present review we summarize the principal concepts and equations which have emerged from this recent research and which provide us with a better framework for understanding many types of reactions, including gas–phase bimolecular and

J. Bertrán and I. G. Csizmadia (eds.),
New Theoretical Concepts for Understanding Organic Reactions, 291–346.

Kluwer, Dordrecht, 1989

unimolecular reactions, reactions on surfaces, and reactions in solution.

As mentioned above, the absolute rate approach requires information about the potential energy as a function of nuclear coordinates; the amount of such information required is dependent upon which generalization of TST is used, and whether tunneling corrections are important. For a variational transition state theory calculation with a fully optimized multidimensional tunneling correction, the amount of information required is intermediate between a reaction–path Hamiltonian and a full energy surface.

Although derivations of TST may be found in many textbooks, these derivations are almost invariably based on a quasi–thermodynamic treatment of a postulated equilibrium between the reactant and transition state species [1,3]. One can obtain more insight into the validity of the theory, though, by deriving it from a dynamical approach [4–8], which makes the nature of the equilibrium assumption more transparent. This type of derivation, which we shall use here, allows for an explicit statement of the dynamical assumptions required by TST. It also provides a specific definition of the transition state "species", and — it will be seen — this definition naturally allows for variational improvements of TST. We will derive a result for generalized transition state theory (GTST), and we will obtain conventional and variational TST as special cases.

Section 2 contains a pedagogically oriented dynamical derivation of TST. We begin this section by defining a useful general coordinate system. Then we consider the continuity equation for an ensemble of reactive systems in phase space, and we present a simple derivation of an expression for the equilibrium flux through a phase–space hypersurface that divides reactants from products. We equate this hypersurface with the transition state species, and we make the TST approximation, which equates this flux to the rate constant. We end Section 2 by showing the equivalence of the dynamical result with the standard result derived by postulating the transition state to be in equilibrium with reactants. All considerations in Section 2 are entirely classical. In Section 3 we quantize all modes except the reaction coordinate, and in Section 4 we describe several methods for including quantum effects on the reaction coordinate.

Section 5 discusses tests and applications of the theory to various gas–phase processes, and Section 6 discusses extensions to reactions at crystalline surfaces and in condensed phases.

In Section 7 we discuss different ways to formulate GTST in terms of quasi–thermodynamic parameters of the transition state species. We show that nonconventional contributions to the enthalpy and entropy of the transition state species may be required in order to use these quantities to accurately estimate rate constants.

2. Classical Variational Transition State Theory

First we derive a classical generalized transition state theory rate constant expression, following Refs. 4–8. We consider, as a general example, a system of classical particles which interact according to a known energy surface V. Specifically, we consider systems in which reaction occurs electronically adiabatically in the ground electronic state with negligible vibronic coupling. The reaction may then be treated as the motion of N atoms governed by a single Born–Oppenheimer potential energy surface. We consider an N–atom system which can undergo chemical bond rearrangement. This system will be, at any

given time, in the reactant region of phase space, in the product region, or in some intermediate region. If the reaction is to be described unambiguously, the probability of being in the intermediate region should be small.

We shall consider both bimolecular and unimolecular reactions. In the former case we write

$$A + B \rightarrow AB^{\ddagger} \rightarrow P, \tag{1}$$

where A and B represent the reactant species, which may be atoms, radicals, molecules, or ions, $AB^{\ddagger}$ represents an activated complex, and P represents the products, which may be an associated product AB or two new subsystems, say C and D. In the case of unimolecular reactions, we write

$$A \rightarrow A^{\ddagger} \rightarrow P. \tag{2}$$

In both (1) and (2) we pay no explicit attention to inert collision partners or solvents, although these may play an essential role in promoting equilibrium among reactants, stabilizing nascent products, or both. If collision partners or solvents have interactions with the reactants or with the activated complex that alter the partition functions of these reacting species, they can be included by letting A, B, and $AB^{\ddagger}$ or A and $A^{\ddagger}$ represent solvated species rather than isolated ones.

Before deriving the classical transition state theory formalism for treating such reactions, we present the coordinate system we use to describe N–atom systems. For simplicity we formulate the description of such systems in terms of 3N isoinertial mass–scaled cartesian coordinates [9]. [These are essentially the same as the mass–weighted cartesians widely used in vibrational spectroscopy [10]. The difference is that the spectroscopists' coordinates have units $(\text{mass})^{\frac{1}{2}}$ length, but we introduce an extra factor $\mu^{-\frac{1}{2}}$ so that the coordinates have units of length.] Thus, if $R_{i\gamma}$, for $\gamma = x, y, z$, are the cartesian coordinates of atom i with respect to the center of mass of the system, then the mass–scaled coordinates are defined by

$$q_j = \left(\frac{m_i}{\mu}\right)^{\frac{1}{2}} R_{i\gamma}; \quad i=1,...,N; \quad \gamma=x,y,z; \quad j=1,...,3N, \tag{3}$$

where m_i is the mass of atom i, and μ is a parameter with units of mass. A convenient choice of μ is the one used by spectroscopists, i.e., 1 atomic mass unit (1 u = 1 universal amu based on ^{12}C). Another convenient choice, for gas–phase bimolecular reactions at least, is the reduced mass of reactant relative translational motion,

$$\mu_{rel} = m_A m_B/(m_A + m_B), \tag{4}$$

where m_A and m_B are the masses of reactant A and B, respectively. In the coordinate system of (3), the kinetic energy contains no cross terms, and the

reduced mass μ factors out, i.e.,

$$T = \frac{1}{2}\mu \sum_{i=1}^{3N} \left(\frac{dq_i}{dt}\right)^2, \tag{5}$$

which means that the same mass μ is associated with motion in any direction. (This is why the coordinates are called "isoinertial.") Therefore, motion of the N–atom system governed by the potential surface $V(\{R_{i\gamma}\})$ is equivalent to the motion of a single–particle of mass μ in 3N dimensions governed by the energy surface $V(\{q_i\})$. In other words, if we could construct the 3N–dimensional potential surface, $V(\{q_i\})$, and slide a frictionless point of mass μ along this surface, the position and momentum, $\{q_1(t)...q_{3N}(t), p_1(t)...p_{3N}(t)\}$, of this mass on the surface at any given time t would correlate to the actual configuration and momentum of the many–atom system at time t. Thus the use of mass–scaled coordinates reduces an N–body problem in three dimensions to a 1–body problem in 3N dimensions.

The classical statistical mechanics of the reaction will be treated using an ensemble of N–atom systems, each represented at a given time t by a point $(\vec{p},\vec{q})$ in 6N–dimensional phase space, where $\vec{p} = \mu\, d\vec{q}/dt$. The kinetic and potential energies of the system are functions of the 3N–dimensional vectors defining the phase points, i.e., $T = T(\vec{p})$ and $V = V(\vec{q})$. The Hamiltonian, which is needed below, is given by

$$H(\vec{p},\vec{q}) = T(\vec{p}) + V(\vec{q}). \tag{6}$$

We will derive the classical transition state theory rate constant in two steps. First we will derive an expression for the equilibrium flux of systems passing through a mathematical surface separating reactants from products. Then we will identify this surface with the transition state to reaction and make the fundamental assumption of transition state theory to relate the equilibrium value of the flux through the transition state to the overall reaction rate.

2.1. FLUX THROUGH A SURFACE

Consider an ensemble of systems like the one described in the previous section, each of which is described by a 6N–dimensional point in phase space. Defining the density of classical phase space points as $\rho(\vec{p},\vec{q})$ and the rate of change of this density with time as $(\partial\rho/\partial t)$, it is clear that conservation of the number of phase space points in the ensemble requires the satisfaction of the continuity equation [11,12]

$$\frac{\partial\rho}{\partial t} + \vec{\nabla} \cdot \rho\vec{v} = 0, \tag{7}$$

where $\vec{\nabla}$ is the 6N–dimensional divergence operator [11a] and $\vec{v}$ is the 6N–dimensional velocity of a point in phase space.

Different regions of phase space are governed by different parts of the potential surface $V(\vec{q})$, and, consequently, may correspond to different chemical species. Thus, by following the flow of points between specific regions of phase space, we can study the course of chemical reaction in our ensemble of chemical systems [4,5]. To this end we first consider a volume R in phase space corresponding to the reactants. Rearranging eq. (7) and integrating over the phase space volume R yields

$$-\frac{\partial}{\partial t}\int_R d^{6N}\tau\,\rho = \int_R d^{6N}\tau\,\vec{\nabla}\cdot\rho\vec{v}, \tag{8}$$

where we have introduced the 6N–dimensional volume element

$$d^{6N}\tau = \prod_{i=1}^{3N} dp_i dq_i \tag{9}$$

and we have used the fact that the volume R is not a function of time. Since the integral on the left–hand–side of eq. (8) is just the number N^R of systems in our ensemble that are in the region R, we define the quantity

$$N^R = \int_R d^{6N}\tau\,\rho, \tag{10}$$

and rewrite eq. (8) as

$$-\frac{dN^R}{dt} = \int_R d^{6N}\tau\,\vec{\nabla}\cdot\rho\vec{v}, \tag{11}$$

which clearly shows that the right–hand side counts the number of systems leaving the reactant region of phase space as a function of time.

Next we define S to be a (6N–1)–dimensional surface in phase space which bounds the volume R. We can use Gauss' theorem [11b] to rewrite eq. (11) as a surface integral, i.e.,

$$-\frac{dN^R}{dt} = \int_S da\,\rho\vec{v}\cdot\vec{n}, \tag{12}$$

where da is the differential element of area lying in the surface S, and $\vec{n}$ is a unit vector normal to the surface S and pointing out of the volume R.

Now we define S as a (6N–1)–dimensional hyperplane which divides the reactant region from the product region. We assume that the chemistry of the situation allows us to find a hyperplane dividing reactants from products such that all flux leaving R passes through it. There is then no error incurred in using this hyperplane instead of an enclosing surface to divide reactants from products. In this section, our goal is to calculate the local one–way flux F^+ through this

dividing surface, i.e. the local flux of systems going from reactants to products. Since eq. (12) gives the difference of the local forward flux and the local reverse flux through the dividing surface, i.e. the *net* local flux, we can define F^+ by analogy to eq. (12) as [5]

$$F^+ = \int_{S_+} da\, \rho \vec{v} \cdot \vec{n}, \tag{13}$$

where S_+ is the portion of the dividing surface S for which

$$(\vec{v} \cdot \vec{n}) > 0. \tag{14}$$

When we substitute the equilibrium density for ρ, eq. (12) will of course give zero, but eq. (13) will give the equilibrium one–way flux.

The most convenient way to evaluate F^+ for the specific case described above is to define our coordinates such that q_{3N} is a cartesian coordinate normal to S. This special coordinate is the local reaction coordinate, and it will be called z. The surface is then defined by setting z equal to a fixed value which we denote as z_*. With these definitions, the component of velocity orthogonal to the surface S, in the direction reactants–to–products, is

$$\vec{v} \cdot \vec{n} = \frac{dz}{dt} = \frac{p_z}{\mu} = \frac{p_{3N}}{\mu}. \tag{15}$$

The condition (14) then becomes $\frac{dz}{dt} > 0$ or $p_z > 0$, and the surface element da becomes

$$\begin{aligned} da &= dq_1 \ldots dq_{3N-1} dp_1 \ldots dp_{3N-1} dp_z, \\ &= d^{6N-2}\tau dp_z. \end{aligned} \tag{16}$$

Substitution of eq. (15) and eq. (16) into eq. (13) yields

$$F^+ = \int_{z=z_*} d^{6N-2}\tau \int_0^\infty dp_z\, \rho \frac{p_z}{\mu}. \tag{17}$$

Notice that the limits on dp_z are 0 to ∞, rather than $-\infty$ to ∞, because of eq. (14).

In this section, we shall confine our attention to systems for which it is a good assumption to consider the reactants to be in local equilibrium at a fixed temperature. The validity of this assumption for different types of reactions will be discussed in Section 2.4. In such systems, the density of states is given by a Boltzmann distribution [13],

$$\rho = \rho_0 \, e^{-H/\tilde{k}T}, \tag{18}$$

where H is the classical Hamiltonian of eq. (6), ρ_0 is a constant, $\tilde{k}$ is Boltzmann's constant, and T is the temperature. Substitution of this distribution into eq. (17) yields the one–way flux as a function of temperature,

$$F^+(T) = \rho_0 \int_{z=z_*} d^{6N-2}\tau \int_0^\infty dp_z \, e^{-H/\tilde{k}T} \frac{p_z}{\mu}, \tag{19}$$

while substitution into eq. (10) yields

$$N^R(T) = \rho_0 \int_R d^{6N}\tau \, e^{-H/\tilde{k}T}. \tag{20}$$

In order to perform the integration over dp_z in eq. (19), we separate the Hamiltonian as

$$H = \frac{p_z^2}{2\mu} + H^{GT}(\vec{u},\vec{p}_u;z) \tag{21}$$

where $(p_z^2/2\mu)$ is the kinetic energy associated with motion along z, orthogonal to the surface, and $H^{GT}(\vec{u},\vec{p}_u;z)$ is the remaining part of the Hamiltonian; $\vec{u}$ denotes the coordinates $q_1, q_2, \ldots, q_{3N-1}$, and $\vec{p}_u$ denotes the conjugate momenta $p_1, p_2, \ldots, p_{3N-1}$. (The superscript GT denotes the fact that the fixed–z hyperplane is a generalized transition–state.) Substitution of the separated Hamiltonian, eq. (21), into eq. (19) gives

$$F^+(T) = \rho_0 \int_0^\infty dp_z \frac{p_z}{\mu} e^{-p_z^2/2\mu\tilde{k}T} \int d^{6N-2}\tau \, e^{-H^{GT}(\vec{u},\vec{p}_u;z=z_*)/\tilde{k}T}. \tag{22}$$

Notice that we set $z=z_*$ in H^{GT} because the integral is only over the surface $S(z=z_*)$. Integration over dp_z yields the desired expression for the local one–way flux through a dividing surface,

$$F^+(T) = \rho_0 \tilde{k}T \int d^{6N-2}\tau \, e^{-H^{GT}(\vec{u},\vec{p}_u;z=z_*)/\tilde{k}T}. \tag{23}$$

Since eq. (23) can also be considered to be the one–way flux through a generalized transition state fixed at $z=z_*$, we shall refer to $F^+(T)$ as $F^{GT}(T,z_*)$ from here on.

2.2. FUNDAMENTAL ASSUMPTION OF TRANSITION STATE THEORY

Since the rate of a reaction depends on the concentration of the reactants, it is convenient to work not with the rate itself, as in eq. (12), but rather with the rate coefficient, k(T), which is defined as the reaction rate per unit volume divided by the product of the concentrations of the reactants. For simplicity we now consider the ideal case where back reaction is negligible. Then by "reaction rate" we mean net flux from reactants to products when the product concentration is negligible. Having calculated the rate coefficient for this ideal case, we will assume, as is standard in chemical kinetics, that it may also be used in more complicated circumstances, such as when back reaction or side reactions are not negligible.

We shall consider only gas–phase reactions in this section. The results for reactions in condensed phases, e.g., reactions in solution and reactions on surfaces, will be similar, but in these cases the overall translation of the reactant(s) and the overall translation of the transition state species are not free, i.e. they are hindered by interactions with the bath molecules, and, consequently these degrees of freedom cannot be separated from the rest of the problem, as they are in gas–phase systems.

For a unimolecular reaction [eq. (2)], the rate constant is given by

$$k(T) = \frac{F(T)}{V[A]} \tag{24}$$

where F(T) is the global net reactive flux through the surface bounding the reactant region of phase space, in molecules per unit time and in the absence of products; V is the volume; and [A] is the concentration of the reactant in molecules per unit volume. By the definition of concentration,

$$[A] = N_A/V, \tag{25}$$

where N_A is the number of molecules of the reactant A. For a unimolecular reaction, however, $N_A = N^R(T)$ as defined by eq. (20), and substitution of eq. (25) into eq. (24) will therefore yield

$$k(T) = \frac{F(T)}{N^R(T)}. \tag{26}$$

The local equilibrium one–way flux $F^+(T)$, as given by $F^{GT}(T,z_*)$ in eq. (23), is not, however, necessarily equal to the global net equilibrium flux in the absence of products, as required in eq. (26). In general, if reactants are at equilibrium, $F^{GT}(T,z_*)$ will be greater than F(T), since although all systems contributing to the flux out of the reactant region and into the product region must cross S at least once, there is no guarantee that they will cross S only once. Thus, a system which crosses S towards products and then recrosses S towards reactants will make a positive contribution to the local one–way flux, $F^{GT}(T,z_*)$,

but will not contribute to the net flux, F(T). It is easy to see [14,15] that any trajectory which crosses the dividing surface more than once will make a greater contribution to $F^{GT}(T,z_*)$ than to F(T); thus $F^{GT}(T,z_*)$ provides an upper bound to F(T) if reactant equilibrium is maintained. It is also clear that $F^{GT}(T,z_*)$ will only be a good approximation to F(T) if the dividing surface is defined in such a way that there is little or no recrossing of trajectories before they are thermalized in the reactant or product region, i.e., if the dividing surface is placed at a good bottleneck to reaction.

In order to further evaluate eq. (26), we employ the "last assumption" [4,16] of classical transition state theory, namely that we can find a dividing surface S(z) for which there is no recrossing and the local one–way flux $F^{GT}(T,z_*)$ equals the global net flux, F(T). (By "no recrossing" we mean that all paths crossing the surface toward products originate in R and cross S only once, ending in the product region of intrest [4].) If we then substitute eq. (23) into eq. (26), we obtain the classical generalized transition state theory rate constant $k_C^{GT}(T)$ as

$$k_C^{GT}(T) = \frac{\rho_0 \tilde{k}T \int d^{6N-2}\tau \, e^{-H^{GT}(\vec{u},\vec{p}_u;z=z_*)/\tilde{k}T}}{N^R(T)}, \tag{27}$$

where the superscript GT again denotes the fact that the fixed–z hyperplane is a generalized transition state.

In order to further understand the expression for the GTST rate constant, eq. (27), it is useful to consider the general classical partition function for a system of N distinguishable particles which is given by [13]

$$Z_C(T) = \frac{1}{h^{3N}} \int d^{6N}\tau \, e^{-H(\vec{p},\vec{q})/\tilde{k}T}, \tag{28}$$

where $H(\vec{p},\vec{q})$ is defined by eq. (6), $d^{6N}\tau$ is defined by eq. (9), and h is Planck's constant. The classical partition function, eq. (28), is effectively a weighted sum of "single–quantum–state cells" in phase space; each cell is a box with volume h^{3N} in 6N–dimensional phase space and is weighted by its probability of being populated; the weighting factor is given by the Boltzmann factor $e^{-H(\vec{p},\vec{q})/\tilde{k}T}$. We also define here the classical partition function per unit volume, $\Phi_C(T)$, which is related simply to $Z_C(T)$ by

$$\Phi_C(T) = Z_C(T)/V, \tag{29}$$

where V is the volume of the system. By comparing eq. (20) to eq. (28), it is clear

that $N^R(T)$ is related to the reactant classical partition function $Z_C^A(T)$ [given by eq. (28), but with the integration restricted to the reactant region of phase space] by

$$N^R(T) = \rho_0 \, h^{3N} \, Z_C^A(T). \tag{30}$$

Comparison of eq. (29) with eq. (30) yields the relation between $N^R(T)$ and the reactant partition function per unit volume, $\Phi_C^A(T)$, as

$$N^R(T) = \rho_0 \, h^{3N} \, V \, \Phi_C^A(T). \tag{31}$$

The integral in the numerator in eq. (27) can also be related to a classical partition function. In particular, consider the partition function per unit volume, $\tilde{\Phi}_C^{GT}$ (where the tilde implies a specific zero of energy as discussed below), for systems which lie in the dividing surface, i.e., for systems which have a fixed value of $z=z_*$. Because $\tilde{\Phi}_C^{GT}$ encompasses only (3N–1) degrees of freedom, and is therefore not a partition function for any real species, it may be called a quasi–partition function [17,18]. Specifically, keeping 1 degree of freedom fixed in eqs. (28) and (29) leads to the defining relation for $\tilde{\Phi}_C^{GT}(T,z_*)$,

$$\tilde{\Phi}_C^{GT}(T,z_*) = \frac{1}{Vh^{(3N-1)}} \int d^{6N-2}\tau \, e^{-H^{GT}(\vec{u},\vec{p}_u;z=z_*)/\tilde{k}T}. \tag{32}$$

Computationally it is not convenient to define this quasi–partition function for the transition state "species" from the reactant zero of energy as in eq. (32). Instead we define a quasi–partition function $\Phi_C^{GT}(T,z_*)$ which has as its zero of energy the potential energy, $V_{RP}(z=z_*)$, of the reaction path at the point where the reaction path intersects the generalized transition state surface. (If no reaction path has been defined, we take the intersection point as the point of lowest energy in the hyperplane.) Thus $\Phi_C^{GT}(T,z_*)$ is related to $\tilde{\Phi}_C^{GT}(T,z_*)$ by

$$\Phi_C^{GT}(T,z_*) = e^{V_{RP}(z=z_*)/\tilde{k}T} \, \tilde{\Phi}_C^{GT}(T,z_*). \tag{33}$$

Combining eqs. (32) and (33) and rearranging gives

$$\int d^{6N-2}\tau\, e^{-H^{GT}(\vec{u},\vec{p}_u;z=z_*)/\tilde{k}T} = h^{(3n-1)}V\Phi_C^{GT}(T,z_*)e^{-V_{RP}(z=z_*)/\tilde{k}T} \tag{34}$$

Finally, substitution of eq. (31) and eq. (34) into eq. (27) gives the transition state theory rate constant in its quasi–equilibrium form,

$$k_C^{GT}(T,z_*) = \frac{\tilde{k}T}{h}\frac{\Phi_C^{GT}(T,z_*)}{\Phi_C^{A}(T)}e^{-V_{RP}(z=z_*)/\tilde{k}T} \tag{35}$$

Equation (35) may be simplified by canceling out the partition function for overall translation of the whole system in the numerator and denominator. To do this we note that

$$\Phi_C^X = \Phi_{trans}^X Q_C^X, \tag{36}$$

where Q_C^X is the internal partition function (including overall rotation) of X, and Φ_{trans}^X is the translational partition function per unit volume of X given by

$$\Phi_{trans}^X = (2\pi m_X \tilde{k}T/h^2)^{3/2}, \tag{37}$$

where m_X is the mass of X. Since the mass of the transition state species is the same as the mass of the reactant, Φ_{trans} will cancel in the numerator and denominator of eq. (35), yielding

$$k_C^{GT}(T,z_*) = \frac{\tilde{k}T}{h}\frac{Q_C^{GT}(T,z_*)}{Q_C^{A}(T)}e^{-V_{RP}(z=z_*)/\tilde{k}T} \tag{38}$$

We can derive a similar expression for bimolecular reactions by replacing eq. (24) with its bimolecular counterpart,

$$k(T) = \frac{F(T)}{V[A][B]}, \tag{39}$$

and noting that

$$[A][B] = \frac{N_A N_B}{V^2}, \tag{40}$$

which gives, with eq. (39),

$$k(T) = \frac{F(T)V}{N_A N_B}. \tag{41}$$

To continue, we note that in the reactant region, the reactants are independent of each other; consequently the reactant Hamiltonian may be written as

$$H = H_A + H_B, \tag{42}$$

i.e., as the sum of the Hamiltonians of the reactants. We also note that H_A is a function of $\{q_{1,A},\ldots,q_{3n_A,A}; p_{1,A},\ldots,P_{3n_A,A}\}$ and that H_B is a function of $\{q_{1,B},\ldots,q_{3n_B,B}; p_{1,B},\ldots,p_{3n_B,B}\}$, where $3n_X$ is the number of degrees of freedom for reactant X, and the union of these two sets of coordinates is equivalent to the set $\{q_1,\ldots,q_{3N}; p_1,\ldots,p_{3N}\}$. We can then write the denominator of eq. (41) as

$$N_A N_B = \rho_o \int_R e^{-H_A/\tilde{k}T} dq_{1,A}\ldots dq_{3n_A,A} dp_{1,A}\ldots dp_{3n_A,A} \times$$
$$\times \int_R e^{-H_B/\tilde{k}T} dq_{1,B}\ldots dq_{3n_B,B} dp_{1,B}\ldots dp_{3n_B,B}, \tag{43}$$

which is related to the product of the reactants' classical partition functions per unit volume Φ_C^A and Φ_C^B by

$$N_A N_B = \rho_o h^{3n_A} V\Phi_C^A(T)\, h^{3n_B} V\Phi_C^B(T). \tag{44}$$

Making the TST assumption, we replace F(T) with $F^{GT}(T,z_*)$ in eq. (41). Using eq. (34) to write $F^{GT}(T,z_*)$ in terms of partition functions and eq. (44) for $N_A N_B$, eq. (41) yields

$$k_C^{GT}(T,z_*) = \frac{\tilde{k}T}{h} \frac{\Phi_C^{GT}(T,z_*)}{\Phi_C^A(T)\Phi_C^B(T)} e^{-V_{RP}(z=z_*)/\tilde{k}T}, \tag{45}$$

where we used the fact that $N = n_A + n_B$. In order to use eq. (36) to separate out

the overall translation from $\Phi_C^{GT}(T,z_*)$, $\Phi_C^{A}(T)$, and $\Phi_C^{B}(T)$, we note that the mass for the transition state species is $M = m_A + m_B$, where m_A and m_B are the masses of reactant A and B, respectively. Using eq. (37), we find the ratio of translational partition functions to be

$$\frac{\Phi_{trans}^{GT}(T)}{\Phi_{trans}^{A}(T)\Phi_{trans}^{B}(T)} = \frac{1}{\Phi^{rel}(T)} = \left[\frac{h^2}{2\pi\mu_{rel}\tilde{k}T}\right]^{3/2}, \tag{46}$$

where μ_{rel} is defined in eq. (4), and $\Phi^{rel}(T)$ denotes the reactants' relative translational partition function per unit volume. We define a reactant partition function per unit volume, $\Phi_C^{R}(T)$ as

$$\Phi_C^{R}(T) = \Phi^{rel}(T)Q_C^{A}(T)Q_C^{B}(T), \tag{47}$$

and eq. (45) the rate for a bimolecular reaction becomes

$$k_C^{GT}(T,z_*) = \frac{\tilde{k}T}{h}\frac{Q_C^{GT}(T,z_*)}{\Phi_C^{R}(T)}e^{-V_{RP}(z=z_*)/\tilde{k}T}. \tag{48}$$

To this point, we have considered only systems having a single reaction path. To account for reaction path multiplicity, we need only multiply eq. (48) [or eq. (38) for a unimolecular reaction]) by a symmetry factor, σ, which is determined by the number of equivalent reaction paths [19]. For example, the reaction OH + H_2 would have $\sigma = 2$, since either atom of the H_2 molecule could be abstracted. Thus, the rate is given by [17]

$$k_C^{GT}(T,z_*) = \sigma\frac{\tilde{k}T}{h}\frac{Q_C^{GT}(T,z_*)}{\Phi_C^{R}(T)}e^{-V_{RP}(z=z_*)/\tilde{k}T} \tag{49a}$$

for a bimolecular reaction, and by

$$k_C^{GT}(T,z_*) = \sigma\frac{\tilde{k}T}{h}\frac{Q_C^{GT}(T,z_*)}{Q_C^{A}(T)}e^{-V_{RP}(z=z_*)/\tilde{k}T} \tag{49b}$$

for a unimolecular reaction. When reaction path multiplicity is included in $k_C^{GT}(T,z_*)$ as in eq. (49), the rotational partition functions in $Q_C^{GT}(T,z_*)$, $\Phi_C^{R}(T)$, and $Q_C^{A}(T)$ should not include any symmetry factors [19].

2.3. CHOICE OF DIVIDING SURFACE

Because the degree to which the TST rate constant approximates the true rate constant is determined by the amount of recrossing of the dividing surface, and, therefore, by the precise choice of dividing surface, we discuss here a practical method [8,9] for choosing the dividing surface that has been used successfully in many applications. This method defines the (6N–1)-dimensional phase space dividing surface to be a (3N–1)–dimensional coordinate-space hyperplane orthogonal to the path of lowest potential energy connecting the reactant configuration to the product configuration. This path is loosely termed the reaction coordinate; more specifically it is known as the minimum energy path (MEP). The MEP is found from the potential energy surface by starting at the saddle point configuration, which is a maximum along the reaction coordinate but a minimum in the remaining 3N–1 dimensions, and following the path of steepest descents through the mass–scaled coordinate system [20–24]. (One would get a different path if one followed the same procedure in unscaled cartesians [22].) Computational details of the steepest descents procedure may be found elsewhere [17,25,26]. We now find it useful to characterize motion of the system along the MEP by the parameter s; s=0 defines the saddle point, s is negative on the reactant side of the saddle point, and it is positive on the product side. Now, at any given point s, we can rotate and translate our coordinate system such that one rotated coordinate, denoted z, is tangent to the MEP at s and is defined to have a value of zero at the point of tangency. The remaining rotated and translated coordinates $\{q_1(s),...,q_{3N-1}(s)\}$ are orthogonal to the MEP (at s), and the set of all rotated and translated coordinates are called the local natural collision coordinates. We also define the momenta $\{p_1,...,p_{3N-1},p_z\}$ conjugate to the coordinates $\{q_1,...,q_{3N-1},z\}$ at each value of s. Thus, although the MEP may follow a curvilinear path in coordinate space, we have defined, at each value of s, a cartesian coordinate system that has one coordinate tangent to the MEP, i.e., lying along the MEP at s [8,9,17]. Using this coordinate system, any surface in the family of surfaces orthogonal to the MEP may be described by setting $z_* = 0$. The position of a particular surface along the MEP, however, will be determined by the value of the parameter s at which the dividing surface intersects the MEP. The classical TST rate constant of eq. (49) is thus a function of the parameter s, and, for a bimolecular reaction

$$k_C^{GT}(T,s) = \sigma \frac{\tilde{k}T}{h} \frac{Q_C^{GT}(T,s)}{\Phi_C^R(T)} e^{-V_{MEP}(s)/\tilde{k}T}, \qquad (50a)$$

while for a unimolecular reaction

$$k_C^{GT}(T,s) = \sigma \frac{\tilde{k}T}{h} \frac{Q_C^{GT}(T,s)}{Q_C^A(T)} e^{-V_{MEP}(s)/\tilde{k}T}, \qquad (50b)$$

where $V_{MEP}(s)$ is the value of the energy surface on the MEP at s.

The classical conventional transition state theory rate constant $k_C^{\ddagger}(T)$ is obtained from eq. (50) by setting s = 0, i.e., by placing the dividing surface at the saddle point. Note that $V_{MEP}(s=0)$ is just the barrier height for the reaction, and $Q_C^{\ddagger}(T) = Q_C^{GT}(T,s=0)$ is just the quasi–partition function for the saddle point species.

Because the TST rate constant provides an upper bound to the true equilibrium rate constant [$F^{GT}(T,s) \geq F(T)$], a better approximation than $k_C^{\ddagger}(T)$ may be achieved by variationally minimizing $k_C^{GT}(T,s)$ with respect to the surface position, s. This method is called canonical variational transition state theory (CVTST) or, for short, canonical variational theory (CVT). The optimized surface position s_*^{CVT} is defined by the implicit equation

$$k_C^{CVT}(T) = k_C^{GT}(T,s_*^{CVT}) = \min_s k_C^{GT}(T,s), \tag{51a}$$

or, equivalently, by the condition

$$\frac{\partial}{\partial s}\left[k_C^{GT}(T,s)\right]\Big|_{s=s_*^{CVT}} = 0. \tag{51b}$$

The CVT rate constant is then [8,9,17]

$$k_C^{CVT}(T) = \sigma \frac{\tilde{k}T}{h} \frac{Q_C^{CVT}(T)}{\Phi_C^R(T)} e^{-V_{MEP}^{CVT}/\tilde{k}T} \tag{52a}$$

for a bimolecular reaction and

$$k_C^{CVT}(T) = \sigma \frac{\tilde{k}T}{h} \frac{Q_C^{CVT}(T)}{Q_C^A(T)} e^{-V_{MEP}^{CVT}/\tilde{k}T} \tag{52b}$$

for a unimolecular reaction, where $V_{MEP}^{CVT} = V_{MEP}(s = s_*^{CVT})$ and $Q_C^{CVT}(T) = Q_C^{GT}(T,s=s_*^{CVT})$.

By re–writing eq. (50) in a quasi–thermodynamic form, and applying the CVT minimization criteria, eq. (51), we can shed light on the physical meaning of the minimization process [8,17,18,27,28]. For this purpose, although eq. (50) has been derived entirely from dynamical considerations, we re–analyze it in terms of

quasi–thermodynamic parameters. Recalling the statistical expression

$$K = \sigma \frac{Q_B(T)}{Q_A(T)} e^{-\Delta E/\tilde{k}T}, \tag{53}$$

where σ is a symmetry factor, $Q_A(T)$ and $Q_B(T)$ are partition functions for systems A and B, respectively, ΔE is the difference between the zeros of energy for these two systems, and K is the equilibrium constant, allows us to equate the terms

$$K^{GT} = \sigma \frac{Q_C^{GT}(T,s)}{\Phi_C^R(T)} e^{-V_{MEP}(s)/\tilde{k}T} \tag{54a}$$

or

$$K^{GT} = \sigma \frac{Q_C^{GT}(T,s)}{Q_C^A(T)} e^{-V_{MEP}(s)/\tilde{k}T}, \tag{54b}$$

where K^{GT} is referred to as a quasi–equilibrium constant because $Q_C^{GT}(T,s)$ is not the partition function for a real species; rather, it is the partition function for a fictitious species which excludes one degree of freedom. Thermodynamics allows us to write

$$K^{GT} = K^0 e^{-\Delta G_T^{GT,0}(s)/RT} \tag{55}$$

where K^0 is the reaction quotient evaluated at the standard state concentration of each species, i.e., $[AB^{\ddagger}]^0/[A]^0[B]^0 = ([A]^0)^{-1}$ for (1) or $[A^{\ddagger}]^0/[A]^0 = 1$ for (2), and has the same units as K^{GT}, R is the ideal gas constant, and $\Delta G_T^{GT,0}$ is the standard–state molar free energy change between the reactant and transition state species. Like K^{GT}, the free energy, $\Delta G_T^{GT,0}$, is a quasi–thermodynamic quantity, since the transition state species excludes one degree of freedom; it will be called the standard–state generalized free energy of activation. Finally, equating the right–hand sides of eq. (54) and (55) allows us to re–write eq. (50) as [8]

$$k_C^{GT}(T,s) = \frac{\tilde{k}T}{h} K^0 e^{-\Delta G_T^{GT,0}(s)/RT}. \tag{56}$$

Applying the CVT criteria, eq. (51), to eq. (56) yields

$$0 = \left.\frac{\partial k_C^{GT}(T,s)}{\partial s}\right|_{s=s_*^{CVT}}$$

$$= \frac{\tilde{k}T}{h} K^0 \frac{\partial}{\partial s}\left[e^{-\Delta G_T^{GT,0}(s)/RT}\right]\Bigg|_{s=s_*^{CVT}}. \qquad (57)$$

It is clear from eq. (57) that, since the only surface–dependent quantity on the right–hand side is $\Delta G_T^{GT,0}(s)$, the position of the surface along the reaction coordinate which minimizes the canonical rate constant, defined by $s = s_*^{CVT}$, occurs at the position of the maximum of the free energy of activation curve $\Delta G_T^{GT,0}(s)$. Thus, a major difference between conventional TST and CVT is that in CVT a combination of entropic and energetic effects ($\Delta G_T^{GT,0}$) is considered when choosing which dividing surface will best act as a dynamical bottleneck, i.e., which surface will best satisfy the condition that every system which crosses the dividing surface does so only once; whereas, in conventional TST only energetic effects [$V_{MEP}(s=0)$] are considered in making this choice.

The discussion in this section has considered only a one–parameter sequence of hyperplanes perpendicular to s in mass–scaled coordinates. We close this section by considering two aspects of this restriction. First we note that such a hyperplane will not always divide reactants from products everywhere. Second we note that $Q_C^{GT}(T,s)$ is primarily sensitive to the shape of the potential near the reaction path, especially at low and moderate temperatures. We can then see how such a hyperplane could still provide a good estimate of the rate by imagining a true dividing surface that coincides with the orthogonal hyperplane in the vicinity of the reaction path but elsewhere, in regions that do not have a large effect on $Q_C^{GT}(T,s)$, curves into a high–energy region that divides reactants from products (unlike the hyperplane) [29]. This is the basis for the "Morse I" approximation [8,9] in which a vibrational potential orthogonal to the MEP is treated as increasing monotonically to a very high value on one side of the MEP and as increasing monotonically to the bond dissociation limit on the other, even though the true potential along the straight–line vibrational coordinate may not be so well behaved. Of course if vibrational partition functions are calculated harmonically one doesn't need to worry about these details.

Finally we consider the idea that more general dividing surfaces could be used to improve calculated rate constants. If one considers arbitrary variations of the dividing surface in phase space one should be able to obtain the exact classical equilibrium rate constant [4,5]. However this would be practical only for very simple systems, and even for systems with only three atoms it can be very complicated (and has never been carried out completely). Instead, we consider the simple one–parameter sequences of dividing surfaces discussed above, and we note, quite happily, that, even when quantum effects are incorporated by the

approximate methods discussed in Sections 3 and 4, one can obtain quite accurate results in many cases by using such simple prescriptions for the set of trial dividing surfaces over which minimization of the GTST rate coefficient is carried out [29–35].

2.4. VALIDITY OF REACTANT EQUILIBRIUM ASSUMPTION

The validity of the assumption of reactant equilibrium depends upon the ability of some energy transfer mechanism, such as collisions, to repopulate reactive elements of phase space at a rate at least as fast as the rate at which these states are depopulated by reaction. The conditions under which this assumption is valid for unimolecular gas–phase reactions have been widely studied; these conditions are usually called the high–pressure limit [36–38]. (This is a misnomer; actually it is a high–pressure plateau since new effects arise at ultrahigh pressures and in condensed media; see Section 6.) However, at typical pressures where gas–phase unimolecular reactions are studied, thermalization of the reactant states is usually incomplete and the rate is correspondingly lower than the value calculated under the equlibrium assumption. This is called the fall–off regime. In order to calculate accurate rate coefficients in this regime, one usually uses a mechanism including activating collisions, such as the Lindemann mechanism, for which, of course, the rate coefficients are no longer expressed in unimolecular form. For gas–phase bimolecular reactions it is usual to assume that activating collisions are efficient enough to maintain a thermal distribution of reactants, but the extent to which the breakdown of this assumption affects measured rate constants is not well understood. The most complete study available is that of Lim and one of the authors [39]. In condensed phases thermalizing collisions with the solvent are very frequent, but recent research shows that the thermalization of reactants is nevertheless not always assured, and, in addition, in condensed phases and very high–pressure gases one must consider frictional effects that may slow the rate constant by preventing a spatial equilibrium of reactants or interrupting the traversal of the transition state region [2,18,40]. If we refrain from treating low–pressure unimolecular reactions, and we assume reactant equilibration is perfect in other cases, then we may also assume without further error that equilibrium is maintained for species in the transition state dividing surface that originated in the reactant region of phase space. In classical mechanics, in the absence of trajectories trapped in the interaction region, i.e., trajectories that never emerge as reactants or products, this is a direct consequence [41] of Liouville's theorem [12a,42]. Further discussion of the equilibrium assumption of TST is given in Ref. 7. We note that once quantal effects are introduced it is not possible to justify TST so clearly, and eventually our confidence in the theory must be based on checking the computed rate constants against more accurate dynamical calculations and/or experiments. Such tests are discussed further in Refs. 2, 15, and 29–35 and in Section 5.

3. Semiclassical Canonical Rate Constants with Classical Reaction–Coordinate Motion.

Our treatment, up to this point, of both "exact" and transition state theory rate constants has been entirely classical. Yet for most systems quantum effects, especially vibrational zero–point effects and tunneling effects, are quite important.

Because the transition state theory formulation requires the simultaneous knowledge of the reaction coordinate position, z(s), and the corresponding momentum, p_z, and because this simultaneous knowledge is forbidden by the uncertainty principle of quantum mechanics, there is no unique way to rigorously quantize the classical TST result [43]. Instead it is common to use a semiclassical treatment which includes adiabatic quantization of all modes except the reaction coordinate [30,44,45]. In this context, "adiabatic" means that, at each value of s, energy levels are computed for degrees of freedom orthogonal to the reaction coordinate by deleting the kinetic energy in s and fixing s in the potential energy. In addition, in some cases one adds a separate correction for tunneling, which is the dominant nonclassical effect on the reaction coordinate, or at least the dominant one that is conveniently included in TST [15,29–31]. Thus, we separate the quantized generalized transition state rate constant into two factors as

$$k^{GT/G}(T,s) = \kappa^{GT/G}(T,s)k^{GT}(T,s), \tag{58a}$$

where $k^{GT}(T,s)$ is the semiclassical rate constant which includes quantization of all modes except the reaction coordinate, and $\kappa^{GT/G}(T,s)$ is a correction factor used to incorporate quantal effects on the reaction coordinate. The /G in the superscript denotes that a ground–state transmission coefficient method is used to evaluate this correction factor. In this section we will discuss $k^{GT}(T,s)$ and show how to use it to calculate the canonical variational theory rate coefficient $k^{CVT}(T)$. The evaluation of $\kappa^{GT/G}(T,s)$ will be discussed in Section 4 for the special case where CVT is used, and it becomes $\kappa^{CVT/G}(T)$.

Because we invoke a nonrigorous quantization in determining $k^{GT}(T,s)$, and because this quantization is applied only to selected modes, the semiclassical TST rate constant, $k^{GT}(T,s)$, does not provide a rigorous upper bound to the exact quantum rate constant the way the classical TST rate constant $k_C^{GT}(T,s)$ provides an upper bound to the exact classical rate constant. Nevertheless, we have found that variationally optimizing rate constants which have been quantized using this semiclassical scheme yields better numerical results than simply placing the dividing surface at s = 0 [2,15,29–35].

The modes which are quantized in the semiclassical treatment appear in eq. (50) only in the ratio $Q_C^{GT}(T,s)/\Phi_C^R(T)$ for a bimolecular reaction and $Q_C^{GT}(T,s)/Q_C^A(T)$ for a unimolecular one. Thus, eq. (50) can be converted to its semiclassical analog simply by replacing the classical canonical partition functions with their quantum mechanical analogs, i.e.,

$$k^{GT}(T,s) = \sigma \frac{\tilde{k}T}{h} \frac{Q^{GT}(T,s)}{\Phi^R(T)} e^{-\beta V_{MEP}(s)} \qquad \text{(bimolecular)}, \tag{59a}$$

$$k^{GT}(T,s) = \sigma \frac{\tilde{k}T}{h} \frac{Q^{GT}(T,s)}{Q^{A}(T)} e^{-\beta V_{MEP}(s)} \qquad \text{(unimolecular)}, \tag{59b}$$

where $Q^{GT}(T,s)$ and $Q^{A}(T)$ are quantum partition functions, $\Phi^{R}(T)$ is a quantum partition function per unit volume and $\beta = 1/\tilde{k}T$. We make two major assumptions in this semiclassical treatment. First, our method of quantization assumes that the reaction coordinate is separable from the other degrees of freedom (i.e., that there is no coupling between the reaction coordinate and any of the other modes). Second, in evaluating the quantum partition functions, $Q^{GT}(T,s)$, $Q^{A}(T)$, and $\Phi^{R}(T)$, we ignore the coupling between the electronic, vibrational, and rotational degrees of freedom so that we can write

$$Q^{GT} = Q^{GT}_{el} Q^{GT}_{vib} Q^{GT}_{rot}, \tag{60}$$

$$Q^{A} = Q^{A}_{el} Q^{A}_{vib} Q^{A}_{rot}, \tag{61}$$

and

$$\Phi^{R} = Q^{A}_{el} Q^{A}_{vib} Q^{A}_{rot} Q^{B}_{el} Q^{B}_{vib} Q^{B}_{rot} \Phi^{rel}. \tag{62}$$

Note that, because translational partition functions are the same in quantum as in classical mechanics, the cancellations leading to eqs. (38) and (48) involving the separation of partition functions for overall translation remain valid in the semiclassical treatment. It has been shown numerically that quantization of the rotational degrees of freedom is generally unimportant, e.g., using classical rotational partition functions instead of quantum ones to evaluate CVT rate constants causes errors of less than 1% for most atom–diatom reactions [27]. For a nonlinear molecule, the classical rotational partition function is given by

$$Q_{rot} = \left[\left(\frac{2\tilde{k}T}{\hbar^2} \right)^3 \pi I_A(s) I_B(s) I_C(s) \right]^{\frac{1}{2}}, \tag{63}$$

where $\hbar$ is Planck's constant divided by 2π, and I_A, I_B, and I_C are the three principal moments of inertia. For Q^{GT}_{rot}, the moments of inertia depend on the position of the generalized transition state along the reaction coordinate s; numerical methods for calculating $I_A(s)I_B(s)I_C(s)$ have been described elsewhere [17]. For Q^{A}_{rot} or Q^{B}_{rot}, the moments of inertia are those for the specified reactant species, A or B, i.e., at $s = -\infty$. For linear molecules, the classical rotational partition function is given by

$$Q_{rot} = \frac{2I(s)\tilde{k}T}{\hbar^2}, \tag{64}$$

where again, for Q^{GT}_{rot}, the moment of intertia is a function of s, while for Q^{A}_{rot} and Q^{B}_{rot}, I is the moment of inertia for the specified linear reactant. Note that none of the rotational partition functions contain symmetry factors, as these are already accounted for in the inclusion of reaction path multiplicity [cf. eq. (49)].

When evaluating Q_{vib}, we make the independent–normal–mode approximation, which assumes no mode–mode coupling between vibrational modes. This approximation allows the vibrational partition function to be written as

$$Q_{vib} = \prod_{j=1}^{n_{vib}} Q_{vib,j} , \tag{65}$$

where $Q_{vib,j}$ is the vibrational partition function of mode (normal coordinate) j and n_{vib} is the total number of vibrational modes. Making the simplest vibrational approximation, assuming that the potential along each normal coordinate is harmonic, yields

$$Q_{vib,j} = \frac{e^{-\frac{1}{2}\hbar\omega_j\beta}}{(1 - e^{-\hbar\omega_j\beta})} \tag{66}$$

where ω_j is the frequency for mode j. For Q^{GT}_{vib}, the normal coordinates, and thus, ω_j and $Q^{GT}_{vib,j}$, depend upon the position of the dividing surface, s. Note that the zero of energy for each $Q^{GT}_{vib,j}$ must be $V_{MEP}(s)$ for eq. (66) to be correct. This definition is consistent with the exponential in eq. (59). Numerical methods for determining these quantities as a function of s are given elsewhere [17]. For Q^{A}_{vib} or Q^{B}_{vib}, a standard normal mode analysis of the specified reactant yields the quantities necessary to evaluate eqs. (65) and (66). Although we do not discuss them here, more complex treatments of the vibrations which allow for the anharmonicity of the potential along a given mode in the expression for $Q_{vib,j}$ have been used quite successfully [17]; however, the approximation inherent to eq. (65) is almost always retained.

An important case where anharmonicity effects are essential occurs when there are two low–energy reaction paths separated by a low–energy ridge. This may occur when two first–order saddle points are separated by a second–order saddle point slightly higher in energy [46] or when the minimum–energy path from a first–order saddle point encounters a valley–ridge inflection [47,48]. In such a case one may measure the reaction coordinate along a reference path riding the ridge rather than along the true MEP, and it is necessary to treat at least one vibration orthogonal to the reference path as an anharmonic double–minimum potential. If the valley–ridge inflection point occurs on the reactant side of the saddle point so that the MEP from the transition–state saddle point leads to a saddle point between two "reactant" minima, it may also be necessary to use the double–minimum treatment for reactants. When, however, the ridge separating the reaction paths is high enough and the paths are related by symmetry, one can treat only one of them explicitly and include the other in σ.

Finally, to calculate the reactant electronic partition function, we evaluate the sum over electronic states directly, i.e.

$$Q^A_{el} = \sum_\alpha d^A_\alpha e^{-\beta\epsilon^A_{el}(\alpha)}, \tag{67}$$

since it often converges after only 1 or 2 terms. In eq. (67) $\epsilon^A_{el}(\alpha)$ is the energy of electronic state α and d^A_α is the degeneracy factor of this electronic state. For many reactions of interest higher order electronic states tend to increase dramatically in energy with motion along the reaction coordinate, and we usually consider reactions for which this is so. For this type of reaction, we need only consider the lowest lying electronic state to calculate Q^{GT}_{el}. Because we define $V_{MEP}(s)$ as the zero of energy for all GT partition functions, the lowest lying electronic state has energy $\epsilon^{GT}_{el} = 0$ and Q^{GT}_{el} reduces to the ground electronic–state degeneracy factor, d^{GT}_1. Although this simplification is usually applicable [49], a few reactions have been treated for which it is not [50,51].

In the present section we contructed the hybrid rate constants [eq. (59)] by starting with an expression derived from the fundamental assumption of classical transition state theory and simply quantizing the partition functions. Another approach, which may be carried out without first neglecting quantization effects and then re–inserting them, is based on the adiabatic theory of reactions [8,17,30,52–56]. Although the adiabatic theory yields considerable insight, it is less general than TST because the flux–through–a–dividing–surface derivation of TST does not require for its validity that modes orthogonal to the reaction path be adiabatic, as required for the adiabatic derivation to be valid.

When there is more than one maximum in the free energy of activation curve, it is usually sufficient to base the calculated rate constant only on the highest one. However, if desired, one may attempt to include more than one maximum by a unified statistical model [17,57,58].

4. Quantum Effects on the Reaction–Coordinate Motion

In the previous section we introduced a semiclassical formalism for incorporating quantum effects into all modes except the reaction coordinate. This yielded a hybrid rate constant, eq. (59). Quantum effects on reaction coordinate motion are also quite important in many reactions [15,22,29–31]; here we introduce several methods for calculating a correction factor which accounts for these effects. The general form of the corrected rate constant will be written as

$$k^{CVT/G}(T) = \kappa^{CVT/G}(T) k^{CVT}(T), \tag{58b}$$

where $\kappa^{CVT/G}$, the correction factor, or transmission coefficient, depends on the

method (here CVT) used to calculate the hybrid rate constant, as well as on the method used to incorporate the reaction–coordinate quantum effects. The /G in the superscripts denotes that the correction factor is based on the reaction probability of the ground (G) state of reactants.

First consider the artificial case in which the reaction coordinate is separable; then reaction–coordinate motion is one–dimensional motion over a potential barrier. Classically, only those reactants with energy $E > V_B$, where V_B is the barrier height, will cross the barrier to products, thus the classical transmission probability P_C is given by

$$P_C = \Theta[E - V_B], \tag{68}$$

where the Heaviside step function Θ is defined as

$$\Theta(y) = \begin{cases} 0; & y < 0; \\ 1; & y \geq 0. \end{cases} \tag{69}$$

In quantum mechanics, however, there is a finite probability that reactants with energy less than V_B will proceed to products (tunneling) and also a finite probability that reactants with energy greater than V_B will not react (non–classical reflection [59]). If we could find the quantum transmission probability $P^G(E)$, we could calculate the correction factor as

$$\kappa^G(T) = \frac{\int_0^\infty P^G(E) e^{-\beta E} dE}{\int_0^\infty P_C(E) e^{-\beta E} dE}, \tag{70}$$

which is the ratio of the thermal averages of the quantum and classical transmission probabilities for the ground state of reactants (if the reaction–coordinate were separable these probabilities would be independent of the state of the reactants). If eq. (70) is to provide a reasonable model for the correction factor to CVT, the barrier height used to evaluate $P_C(E)$, eq. (68), must be consistent with the hybrid semiclassical scheme used in Section 3 [eq. (58)]; thus $P_C(E)$ is also dependent on the form of GTST being used, and, for clarity we re–write eq. (70) as

$$\kappa^{CVT/G}(T) = \frac{\int_0^\infty P^G(E) e^{-\beta E} dE}{\int_0^\infty P_C^{CVT/G}(E) e^{-\beta E} dE}. \tag{71}$$

When the reaction coordinate is not separable it is not strictly correct to

base the correction factor solely on ground–state transmission probabilities. Nevertheless we will still do so, based on the following arguments. Tunneling effects are primarily important at low temperatures. At these temperatures, the reactant system will be found almost entirely in its ground state or in a state energetically similar to the ground state. For thermoneutral or nearly thermoneutral reactions, this may be true along the entire reaction coordinate; however, for highly exothermic reactions, higher order product states may be energetically accessible even at the low temperatures where tunneling is important, and we should expect that they will often be populated significantly. Although we shall later discuss methods which will be applicable to exothermic reactions involving tunneling directly into an excited state, we shall for now consider only cases where it is reasonable to assume that the system is in the ground state both at the beginning and the end of the tunneling process. (This does not preclude high product vibrational excitation if tunneling occurs early along the MEP, and vibrational nonadiabaticity occurs later.) In this case we replace the quantum transmission probability $P^G(E)$ to be evaluated by our best approximation to the ground state–to–ground–state tunneling probability. For systems with small reaction–path curvature the simplest approximation uses, as the effective potential for the one–dimensional tunneling motion, the adiabatic ground–state one–dimensional potential, $V_a^G(s)$, i.e., we assume that the system remains adiabatically in its ground state along the entire tunneling path [17,22,29,31]. This potential curve is defined as

$$V_a^G(s) = V_{MEP}(s) + \epsilon^G_{int}(s) \tag{72}$$

where $V_{MEP}(s)$ is the value of the potential energy surface at point s on the MEP and $\epsilon^G_{int}(s)$ is the sum of zero point energies for the orthogonal modes at a given s, i.e.,

$$\epsilon^G_{int}(s) = \sum_{j=1}^{n_{vib}} \epsilon^0_{int,j}(s), \tag{73}$$

where $\epsilon^0_{int,j}(s)$ is the ground–state vibrational energy of the j^{th} vibrational mode (rotational modes have no zero–point energy). We also note that to be consistent with CVT, the classical probability must be found using a barrier height of $V_a^G(s_*^{CVT})$, where s_*^{CVT} is the value of s at which the dividing surface is placed to calculate $k^{CVT}(T)$. Thus

$$P_C^{CVT/G} = \Theta[E - V_a^G(s = s_*^{CVT})]; \tag{74}$$

see Fig. 1. Note that the maximum, $\Delta G_T^{CVT,0}$, of the free energy of activation

curve $\Delta G_T^{GT,0}$ occurs at $s = s_*^{CVT}$ [see eq. (56)], which does not usually equal s_*^{AG}, the point where the maximum of $V_a^G(s)$ occurs, since states other than the ground state are included in determining the free energy of activation curve at a nonzero temperature.

Finally, we find that a good compromise between accuracy and efficiency is to use the WKB semiclassical approximation [60,61] to evaluate the approximate ground–state transmission probability, $P^G(E)$. The uniform WKB result for a general, smoothly varying potential barrier, if $E < V_B$, is given by [55,62–64]

$$P(E) = 1/[1 + \exp(2\theta)], \tag{75}$$

where θ, which governs the degree to which the wave function is damped, i.e., the degree to which the transmission probability is decreased by the presence of the barrier, is given by the following imaginary–action integral:

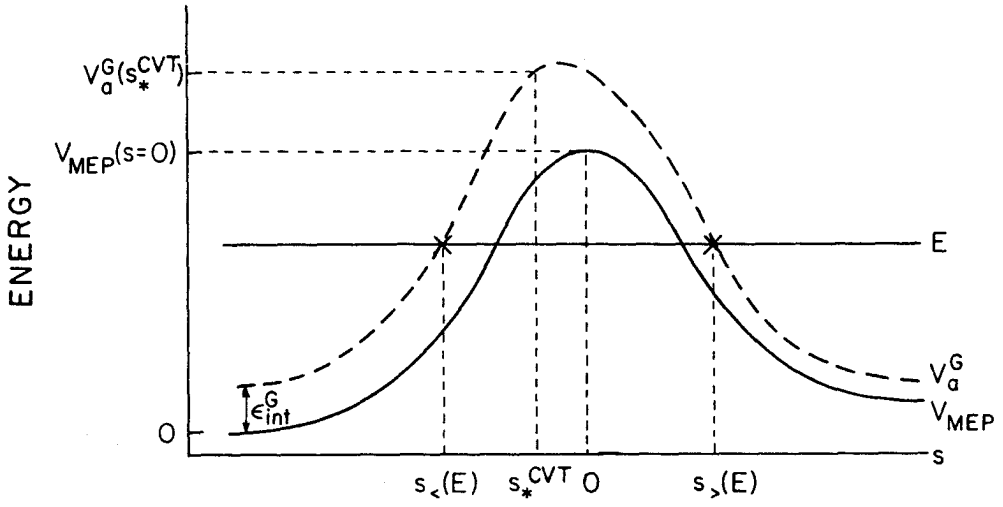

Fig. 1. Potential energy curves as a function of the reaction coordinate parameter s. The solid line represents the potential $V_{MEP}(s)$ along the minimum energy path, and the dashed line represents the adiabatic ground–state potential curve $V_a^G(s)$. The reactant region is at $s = -\infty$, the product region is at $s = +\infty$, the saddle point position is $s = 0$, and a typical generalized transition state position (which is only at the maximum of $V_a^G(s)$ for T = 0 K) is $s = s_*^{CVT}$. The ×'s denote the classical turning points, $s_<$ and $s_>$, for energy E.

$$\theta(E) = \frac{1}{\hbar} \int_{\xi_<}^{\xi_>} \sqrt{2\mu(V(\xi) - E)}\, d\xi, \tag{76}$$

where $\xi_<$, $\xi_>$ are the classical turning points along the tunneling path for energy E, and the integrand is the imaginary part of the tunneling momentum as a function of position. The tunneling momentum can be understood in terms of the following considerations. First, the total energy E is a sum of the local kinetic energy along the tunneling path, $T_{loc}(\xi)$, and the potential energy, $V(\xi)$. This gives

$$T_{loc}(\xi) = E - V(\xi), \tag{77}$$

where ξ denotes the position along the tunneling path. Since tunneling occurs when $E < V(\xi)$, a condition which is satisfied for all $\xi_< < \xi < \xi_>$, the right–hand side of eq. (77) is less than zero, yielding a negative kinetic energy. Converting to momentum, gives

$$\begin{aligned} p(E,\xi) &= \sqrt{2\mu(-|T_{loc}(E,\xi)|)} \\ &= i\sqrt{2\mu|T_{loc}(E,\xi)|} \\ &= i\sqrt{2\mu(V(\xi) - E)}, \end{aligned} \tag{78}$$

showing that the integrand in eq. (76) is indeed the imaginary part of the momentum. It should also be clear from eq. (76) that $\theta(E)$ is a measure of the effective height and width of the barrier. For energies appreciably below the barrier top, θ will be large and eq. (75) will be equivalent to the primitive form [60,61]

$$P(E) \approx \exp[-2\theta(E)], \tag{79}$$

which clearly demonstrates the exponential decay in tunneling probability as a function of barrier height and width.

Returning to the specific problem at hand, the simplest approximation we will consider is called the minimum–energy–path semiclassical adiabatic ground-state tunneling approximation. In this approximation the ground–state tunneling probability is [31,64]

$$P^{MEPSAG}(E) = \{1 + \exp[\tfrac{2}{\hbar} \int_{s_<}^{s_>} [2\mu(V_a^G(s) - E)]^{\frac{1}{2}} ds]\}^{-1}; \quad E < V_a^G(s_*^{CVT}), \tag{80}$$

where we have combined eqs. (75) and (76) and substituted the appropriate values for V and ξ for tunneling through the adiabatic ground state curve, eq. (72). Note

that $s_<$ and $s_>$ are the reaction–coordinate turning points for energy E (see Fig. 1). The probability of equation (80) has the acronym MEPSAG because we have implicitly assumed [22] that the tunneling path passes through the same points in configuration space as does the MEP. Before considering this assumption further, we point out that nonclassical reflection can be treated sufficiently accurately by using a simple relation that is strictly valid only for a parabolic barrier. For a parabolic barrier the probability of reflection at an energy δE above the barrier top is equal to the probability of tunneling at an energy δE below it [62]. Using this to extend eq. (80) we get [17,31]

$$\begin{aligned} P^{\mathrm{MEPSAG}}(E) &= \{1 + \exp[\tfrac{2}{\hbar}\int_{s_<}^{s_>}[2\mu(V_a^G(s) - E)]^{\frac{1}{2}}ds]\}^{-1}; \\ &\qquad V_a^G(s=-\infty) < E < V_a^G(s_*^{\mathrm{CVT}}) \\ &= 1 - P^{\mathrm{MEPSAG}}(2V_a^G(s_*^{\mathrm{CVT}}) - E); \\ &\qquad V_a^G(s_*^{\mathrm{CVT}}) \le E \le 2V_a^G(s_*^{\mathrm{CVT}}) - V_a^G(s=-\infty) \\ &= 1; \\ &\qquad 2V_a^G(s_*^{\mathrm{CVT}}) - V_a^G(s=-\infty) < E. \end{aligned} \tag{81}$$

The replacement of eq. (79) by (81) is called "parabolic uniformization".

Returning to eq. (71), and making use of the Heaviside step function in eq. (74), we have, for the transmission coefficient,

$$\kappa^{\mathrm{CVT/MEPSAG}} = \frac{\int_0^\infty P^{\mathrm{MEPSAG}}(E)e^{-\beta E}dE}{\int_{V_a^G(s_*^{\mathrm{CVT}})}^\infty e^{-\beta E}dE}, \tag{82}$$

or

$$\kappa^{\mathrm{CVT/MEPSAG}} = \beta \exp[\beta V_a^G(s_*^{\mathrm{CVT}})]\int_0^\infty P^{\mathrm{MEPSAG}}(E)e^{-\beta E}dE, \tag{83}$$

where we have performed the integral in the dominator of eq. (82). To correct a CVT rate constant we would use

$$k^{\mathrm{CVT/MEPSAG}}(T) = \kappa^{\mathrm{CVT/MEPSAG}}(T)k^{\mathrm{CVT}}(T). \tag{84}$$

As mentioned previously, the MEPSAG transmission coefficient is calculated under the assumption that the tunneling path follows the MEP. This is a good approximation only for systems having little or no coupling between the

reaction coordinate motion and any of the other degrees of freedom — a situation that seldom occurs. One form of coupling is provided by the curvature of the MEP in mass–scaled coordinates; the vector $\vec{z}(s)$, which is tangent to the MEP at each value of s, will have a different orientation at each value of s. We can illustrate this pictorally for a system having two degrees of freedom — the reaction–coordinate motion plus an additional vibration. Figure 2 depicts such a curved reaction path for a metathesis reaction

$$A + BC \rightarrow AB + C, \tag{85}$$

where A, B, and C may be atoms or groups of atoms. If, for visual purposes, we

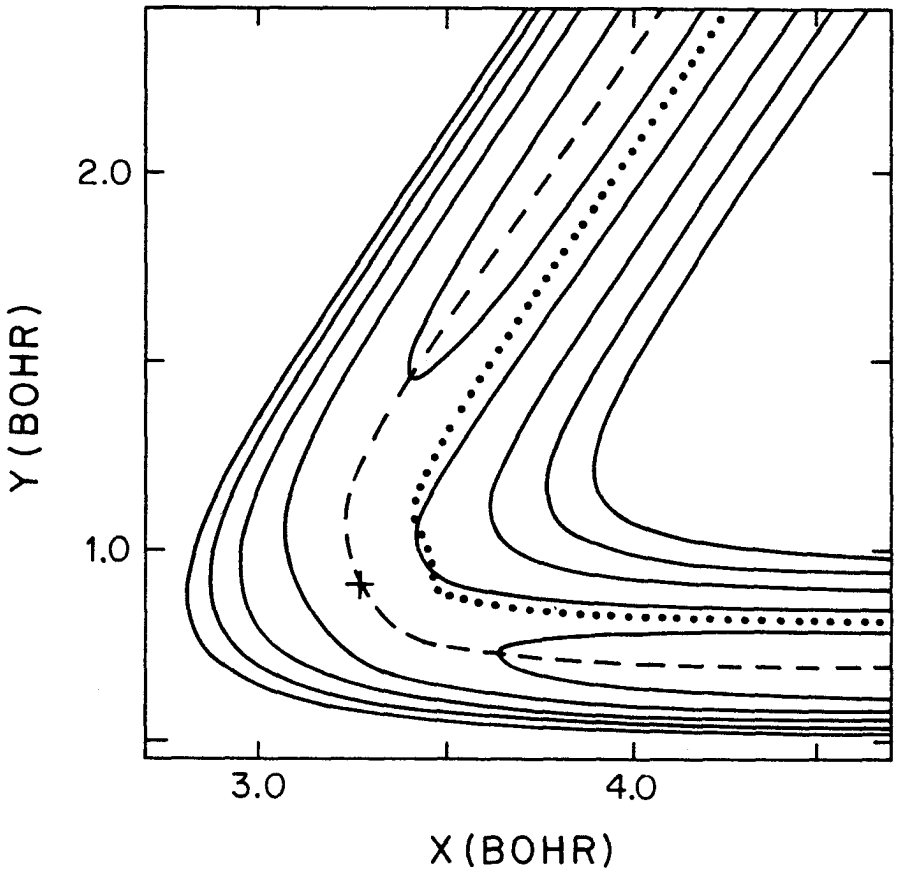

Fig. 2. The potential energy surface of Stern *et al.* [66] for the Cl + DH → ClD + H reaction. The abscissa is the distance from Cl to the center–of–mass of the DH diatom, and the ordinate is the mass–scaled H–D distance. The solid lines represent fixed–energy contours, the dashed line represents the minimum energy path (MEP), the + represents the saddle point, and the dotted line represents the path of classical vibrational turning points when the vibrational motion has zero point energy all along the reaction path.

force this reaction to occur at a fixed A–B–C angle and ignore any internal vibrations in the groups A, B, and/or C, we can plot the potential energy as a function of two coordinates in the mass–scaled system defined by eq. (3). If A, B, and C are all atoms, and we set μ in eq. (3) equal to μ_{rel} of eq. (4), this is equivalent to using two coordinates x and y, where x is the distance from A to the center–of–mass of the BC molecule, and y is a scaled distance from B to C [30] (similar pictures are obtained if one chooses $\mu = 1$ [65]).

Figure 2 is specifically for the medium–curvature system Cl + DH → ClD + H (and the potential energy surface is the GSW surface of Stern *et al.* [66]). The solid lines are potential energy contours, and the dashed line is the MEP. It is known both from analytical semiclassical mechanics [67] and analysis of multidimensional tunneling calculations [68,69] that most of the tunneling flux passes the saddle point on the concave side of the MEP. The dotted curve in Fig. 2 is the path of concave–side classical turning points for the zero point vibrational motion orthogonal to the MEP. For the collinear H + H_2 reaction, Marcus and Coltrin show that this path of turning points is an approximately optimal tunneling path [70]. In the adiabatic ground–state approximation, it is particularly easy to characterize tunneling along this type of shortened path. Because we assume the system is in the ground vibrational state all along the MEP, the classical turning points may be calculated for the vibrational energy $\epsilon^G_{int}(s)$ [eq. (73)]. From this assumption it also follows that the effective potential for tunneling along this path is given by the ground state adiabatic potential curve, $V^G_a(s)$. Thus, the transmission probability for tunneling along this path can be found from eq. (81), as was $P^{MEPSAG}(E)$, except that the coordinate of the tunneling path in the imaginary–action integral of eq. (80) is determined by this shorter path. This is called [31] the Marcus–Coltrin [70] approximation. A generalization of this approach, applicable for any number of atoms and for both collinear and noncollinear MEPs, is accomplished by evaluating the imaginary–action integral along the MEP but replacing the reduced mass μ with an effective reduced mass $\mu^{SC}_{eff}(s)$, which is determined [in the small–curvature (SC) approximation] by the local curvature of the MEP [17,71]. Using this reduced mass is mathematically equivalent to shortening the tunneling path. The transmission probability calculated with this effective reduced mass is called is called $P^{SCSAG}(E)$. This method has been found to give better results than using $P^{MEPSAG}(E)$ for systems with small (but not negligible) amounts of reaction path curvature [29,32]. The small–curvature semiclassical adiabatic ground–state transmission coefficient is given, by analogy to eq. (83), as

$$\kappa^{CVT/SCSAG} = \beta \exp[\beta V^G_a(s^{CVT}_*)] \int_0^\infty P^{SCSAG}(E) e^{-\beta E} dE. \tag{86}$$

We note that for a nonlinear system with 3N degrees of freedom, the reaction-path curvature becomes a vector with as many as 3N–7 nonzero components [72]. These components may be used to define $\mu^{SC}_{eff}(s)$ in the general case [17,71].

For systems with a large amount of reaction path curvature (see Fig. 3), such as group– or atom–transfer reactions for which the exchanged group or atom is much lighter than both the donor and acceptor groups, the small–curvature approximation breaks down [28,46,73,74], and we need another approximation to treat this type of system. This problem has been treated using both hyperspherical [73] and mass–scaled cartesian [17,46,75] coordinates. Here we use the latter approach. In particular we will discuss a scheme which is called the large–curvature ground-state approximation, version 3 (LCG3); this approximation [17,76] is of special interest because it has been defined in such a way as to be particularly easy to apply to general systems with an arbitrary number of degrees of freedom.

Before discussing the LCG3 method, we first consider Fig. 3, which is a potential energy contour diagram in mass–scaled cartesian coordinates for the heavy–light–heavy system $^{37}Cl + D^{35}Cl \rightarrow {}^{37}ClD + {}^{35}Cl$ [46]. The solid lines are

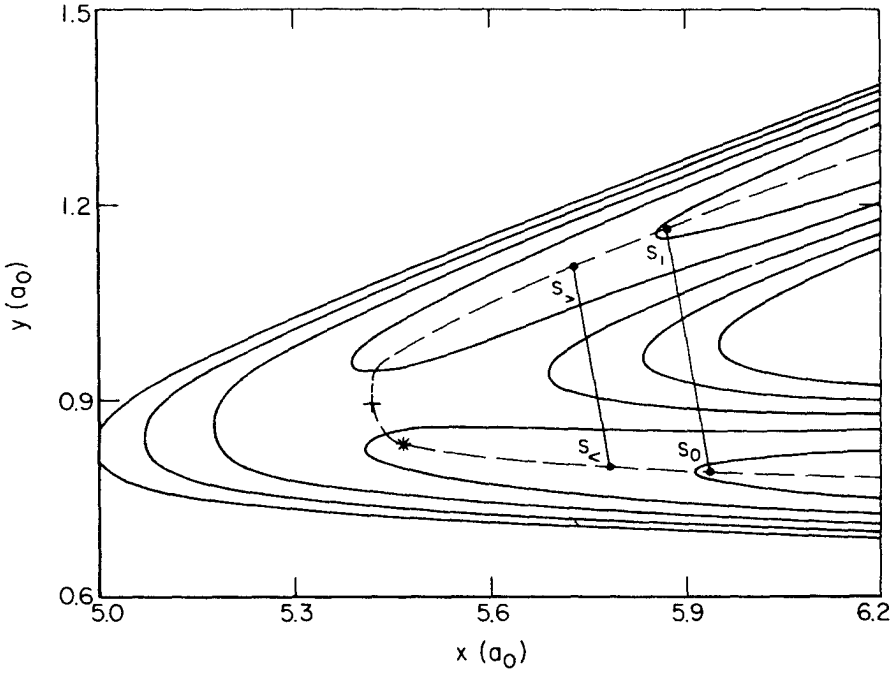

Fig. 3. Potential energy contour diagram for the large curvature system $^{37}Cl + D^{35}Cl$ [46]. The dashed line represents the minimum energy path, + marks the saddle point, and * marks a canonical variational transition state. The points marked $s_<$ and $s_>$ are the classical turning points for reaction–coordinate motion governed by the adiabatic ground–state potential curve $V_a^G(s)$ for energy E, and s_0 and s_1 represent classical turning points for a lower energy and also serve as additional tunneling path termini for energy E. The lines between $s_<$ and $s_>$ and between s_0 and s_1 are typical large–curvature tunneling paths.

the potential contours, the dashed line is the collinear MEP, + represents the saddle point, and * represents the maximum of the adiabatic ground state curve. The fact that the potential contours along a cut perpendicular to the MEP through the saddle point are extremely widely spaced indicates that the vibrational zero point energy is very low at the conventional transition state; this explains why the maximum of $V_a^G(s)$, positioned at a point of higher vibrational zero point energy, is so far removed from the conventional transition state. The saddle point vibrational frequency is low because a symmetric stretch in the heavy–light–heavy case involves only motion of the heavy donor and acceptor atoms. Now consider the reaction-coordinate turning points for some total energy below the maximum of $V_a^G(s)$; these are called $s_<$ for the reactant channel and $s_>$ for the product channel. Due to the curvature of the MEP, the shortest path connecting $s_<$ and $s_>$ has a large component in the direction representing the high–frequency motion of the central light atom, making tunneling from $s_<$ via such a path a highly probable event. We note that the positions of $s_<$ and $s_>$ along the MEP are determined by the total energy of the system and $V_a^G(s)$ (see Fig. 1). For systems with large reaction–path curvature, one finds [46,73–77] that there are also significant tunneling contributions along paths from s_0 to s_1 where $s_0 < s_<$ and $s_1 > s_>$, i.e., the system tunnels before it reaches the entrance–valley reaction-coordinate turning point $s_<$, and the final terminus of the tunneling path is at a point where the reaction–coordinate component of the kinetic energy is greater than zero. The LCG3 approximation includes contributions from all straight–line tunneling paths with equal pre– and post–tunneling reaction–coordinate components of the kinetic energy by using a quasiclassical distribution function to average over tunneling paths with various termini.

Since the degree of exponential damping of the tunneling wave function decreases for lower barriers and for shorter paths, the tunneling amplitude will be largest on the path which provides the best compromise between barrier height and path length. For large–curvature systems, the straight–line paths discussed above, each between a point s_0 in the reactant channel and a point s_1 in the product channel, are so much shorter than the MEP between these points that they yield the dominant tunneling contributions, even though the barriers along these paths are higher than the barrier along the MEP. These paths are shorter, in mass–scaled coordinates, because they involve mostly the motion of the very light central atom. Thus, in this type of system, we calculate the transmission probability by considering only the tunneling along this type of straight–line path. Calculation of the imaginary–action integral, θ [eq. (76)], is more difficult for this type of path, since the effective potential along this path is only given by $V_a^G(s)$ in the regions between the MEP and the classical turning points or between the MEP and the place where vibrational coordinates referenced to the MEP become multivalued. The potential along the rest of this type of path must be calculated from the actual value of the potential energy surface, and it also involves an interpolated value of the zero point energies of modes which are not

curvature–coupled to the reaction coordinate [17,46,75]. In this method, nonclassical reflection is treated by a parabolic uniformization of the MEPSAG action integral.

Since the LCG3 method does not assume adiabaticity throughout the tunneling region, it may be extended to high–barrier or exothermic reactions for which higher product vibrational states are directly populated by the tunneling event (endothermic reactions should be treated in reverse). The contribution to reaction due to tunneling into the various accessible vibrational product states (defined by the quantum number n') is calculated by separately evaluating the contribution for each product vibrational state, and then summing over all of these accessible states. The contributions to the ground vibrational product state are calculated as discussed above, using $V_a^G(s)$ to determine the reaction–coordinate component of the kinetic energy and the quasiclassical distribution function. For each additional available product state, $n' > 0$, we find the tunneling–path terminus $s_{1,n'}$, in the product region, by the relation

$$E_{s_0} = V_{MEP}(s_{1,n'}) + \epsilon_{int}(s_{1,n'},n'), \tag{87}$$

where E_{s_0} is the adiabatic ground–state energy of the system at s_0. We then calculate the tunneling along the straight–line path between s_0 and $s_{1,n'}$. The effective potential used for the calculation along this path is the same as in the general LCG3 method, except in the exit valley, where $V_a(s,n') = V_{MEP}(s) + \epsilon_{int}(s,n')$ is used instead of $V_a^G(s)$. Summation over the individual contributions of the final product states yields the total tunneling probability for this type of reaction [76,77].

Finally, another method has been developed for calculating quantum transmission probabilities which gives results which are similar to SCSAG in the small–curvature limit, similar to LCG3 in the large curvature limit, and of reasonable accuracy for intermediate–curvature systems [32,34,75]. This method, which is called the least–action ground–state approximation (LAG), considers for each pair of tunneling termini a series of tunneling paths ranging from the MEP at one extreme to the LCG3 path at the other. For each energy less than $V_a^G(s_*^{CVT})$, the contribution to the LAG transmission probability, $P^{LAG}(E)$, from each set of termini is given by the tunneling contribution from the path having the largest tunneling probability, i.e., the path giving the smallest imaginary–action integral, θ [eq. (76)]. The contributions from the various pairs of termini are averaged as in the LCG3 method. For the part of any path that is not between the MEP and the classical vibrational turning points or between the MEP and the location on the tunneling path where vibrational coordinates referenced to the MEP become multivalued, the ground–state potential along the path is determined as in the LCG3 method; for the part or parts of any path which are between the MEP and either the path of classical vibrational turning points or the point where local natural collision coordinates break down, $V_a^G(s)$ is used. Thus for each pair of tunneling–path termini the LAG method chooses the best

tunneling path, so that the integral over the quasiclassical distribution function of termini as well as the integral over energy in the expression for the transmission coefficient,

$$\kappa^{CVT/LAG} = \beta \exp[\beta V_a^G(s_*^{CVT})] \int_0^\infty P^{LAG}(E)\, e^{-\beta E}\, dE, \tag{88}$$

encompasses a series of different paths. Again, we incorporate nonclassical reflection into $P^{LAG}(E)$ by making a parabolic uniformization of the MEPSAG tunneling probabilities.

The ability to treat tunneling in high–barrier or exothermic reactions is incorporated into the LAG formalism in the same fashion as described above for the LCG3 formalism. In the LAG method, a best tunneling path is chosen for each pair of termini for each final vibrational product state, n', with the contributions to the various final states being summed at each energy. Again, the only difference in the calculation of the effective tunneling potential along the chosen path is that, in the region between $s_{1,n'}$ and the MEP, $V_a(s,n')$ is used instead of $V_a^G(s)$.

We note that both the LCG3 and the LAG approximations require more information about the potential energy surface than is required for VTST, MEPSAG, or SCSAG calculations. VTST, MEPSAG, and SCSAG calculations require knowledge of the MEP, the potential along the MEP, and the vibrational energies of modes orthogonal to the MEP, but LCG3 and LAG calculations require, in addition, the potential surface in wider swaths on the concave side of the MEP in tunneling regions.

5. Gas–Phase Applications

Sections 2–4 have presented the theoretical formulation of generalized transition state theory and semiclassical tunneling approximations. In order to illustrate the validity and usefulness of this theory for absolute rate calculations we now consider applications to reactions in the gas phase. Although conventional and generalized transition state theory have been applied to many gas–phase systems [33,35], we shall consider only a few examples. Except where stated otherwise, all GTST calculations include anharmonicity by methods discussed elsewhere [8,9,17,31,32,78].

Several studies on collinear atom–diatom reactions have been carried out in which accurate classical mechanical rate constants were calculated for a given energy surface, and these were used to test classical conventional and variational transition state theory. Table I gives some of these results [8,79] for two reactions. For the first reaction, Cl + HD, we see that at 300 K, both the conventional transition state (at $s = 0$) and the canonical variational transition state (at $s = s_*^{CVT}$) provide reasonable bottlenecks, and very little recrossing occurs at either transition state; both $k_C^{\ddagger}$ (300 K) and k_C^{CVT} (300 K) overestimate the accurate rate by only ~10%. At 2400 K, however, recrossing has increased much more

rapidly at the conventional transition state than at the variational one, and $k_C^{\ddagger}$ (2400 K) is nearly twice as large as k_C^{CVT} (2400 K). For the model of an organic hydrogen exchange reaction, R + HR′ → RH + R′, where the alkyl chains R and R′ are represented by carbon atoms having a mass equivalent to that of a butyl radical, the conventional transition state is a poor bottleneck even at as low a temperature as 300 K, while recrossing is so extreme at 2400 K that $k_C^{\ddagger}$ overestimates the accurate classical rate constant by over an order of magnitude. The canonical variational dividing surface, while not providing a perfect bottleneck, yields a rate constant which is high by only a factor of two or less over the whole temperature range. These examples clearly illustrate that the TST approximation — that the local net flux through the transition state, $F^{GT}(T,s)$ [eq. (23)], may be used instead of the global net flux F(T) [eqs. (24) and (39)], to calculate the rate — can be much improved by locating the transition state variationally ($s = s_*^{CVT}$) instead of defining it to be at the saddle point (s = 0).

TABLE I. Ratios of classical transition state theory rate constants to exact classical dynamical ones for two collinear reactions.

Reaction	Temperature, K	‡	CVT
(R1) Cl + HD → ClH + D[a]	300	1.1	1.1
	2400	5.0	2.8
(R2) $^{57}C+H^{57}C' \rightarrow {}^{57}CH+{}^{57}C'$[b]	300	4.3	2.0
	2400	11.4	2.0

[a]Ref. 8.
[b]Ref. 79; three–body model of C_4H_9+H–C_4H_9 → C_4H_9–H+C_4H_9.

In order to show that variational optimization of the transition state can also be important when calculating semiclassical TST rate constants, which no longer provide rigorous upper bounds to the accurate quantum mechanical rate constants, we consider two collinear reactions [29,80–82] for which tunneling effects are negligible; in particular, we consider I + H_2 → IH + H, and I + HI′ → IH + I′, which are called (R3) and (R4), respectively. For (R3) $k^{CVT}(T)$ agrees with $k^{CVT/SCSAG}(T)$ to three significant figures, and for (R4) $k^{CVT}(T)$ agrees with $k^{CVT/LAG}(T)$ to two figures. In these cases we consider the ratios of the semiclassical rate constants to accurate quantal ones for collinear reaction on the same energy surface. As discussed in Section 4, we expect variational effects to be especially important for the heavy–light–heavy mass combination of (R4) because

of the low value of the symmetric stretch frequency at the saddle point for a symmetric reaction with this mass combination. From Table II it is clear that the canonical variational transition state provides a good bottleneck at all temperatures considered for both reactions; $k^{CVT}(T)$ is within 10% of the accurate quantal results at 300–1500 K for the I + H_2 case and within 42% of the accurate results at 100–1000 K for the large–curvature case. The conventional TST results, however, are much worse — $k^{\ddagger}(T)$ overestimates the accurate quantal results for I + H_2 by a factor of 12 at 300 K, while for the more difficult heavy–light–heavy system, $k^{\ddagger}(T)$ overestimates the accurate results by over 4 orders of magnitude at 100 K and by a factor of 57 at 300 K. In general, variational effects (by which we mean the difference of VTST rates from conventional TST ones) may either increase or decrease in importance as the temperature is raised. Increasing importance with increasing temperature is the most common trend in classical calculations, because classical recrossing is more predominant at higher temperatures. This classical trend is typically retained in semiclassical calculations when variational effects are controlled by low–frequency modes. When high–frequency modes are important though, the effects are dominated by zero point energies, and zero point effects decrease with increasing temperature. The reactions in Table II are both examples where high–frequency stretches control the variational effect. The I + HI′ reaction is particularly interesting in this regard. Because the symmetric stretch frequency is so low at the saddle point, the value of the adiabatic ground state curve at the reactants,

TABLE II. Ratios of semiclassical generalized transition state theory rate constants to the accurate quantal ones for two collinear reactions.

Temperature, K	‡	CVT
	(R3) I + H_2 → IH + H[a]	
300	12.1	1.09
600	3.7	1.05
1500	2.1	1.03
	(R4) I + HI′ → IH + I′[b]	
100	1.75×10^4	0.77
300	57.0	1.07
600	21.3	1.22
1000	19.3	1.42

[a]GTST results, Refs. 29 and 30; accurate quantal results, Ref. 80.
[b]GTST results, Ref. 82; accurate quantal results calculated (see Ref. 82) from Ref. 81.

where this mode correlates to a high–frequency hydride vibration, is actually higher than the value of this curve at the saddle point, and the conventional TST rate constant increases with decreasing temperature at temperatures below about 600 K [82]. Consequently, variational effects are most important at low temperatures for this system.

Next we consider rate constants for which tunneling corrections are important. We compare semiclassical CVT rate constants with various transmission coefficients to accurate quantal rate constants, in each case calculated on the same potential energy surface, for 3–dimensional atom–diatom reactions. Table III shows results [34,83–85] for four reactions for which tunneling is quite

TABLE III. Ratios of semiclassical canonical variational transition state theory rate constants (with various transmission coefficients) to accurate quantal rate constants for 3–dimensional atom–diatom reactions.

T,K	CVT	CVT/ MEPSAG	CVT/ SCSAG	CVT/ LCG3	CVT/ LAG
	(R5) $H + BrH' \rightarrow HBr + H'$[a]				
200	0.042	0.59	2.4	1.1	1.5
250	0.14	0.70	1.8	0.98	1.1
300	0.26	0.79	1.6	0.95	0.99
	(R6) $H' + H_2 \rightarrow H'H + H$[b]				
200	0.0018	0.031	0.38	0.59	0.74
250	0.014	0.079	0.51	0.88	0.87
300	0.044	0.15	0.61	1.0	0.92
400	0.15	0.30	0.73	1.1	0.99
	(R7) $O + DH \rightarrow OD + H$[b]				
300	0.14	0.39	1.5	0.84	0.91
400	0.36	0.63	1.4	0.90	0.92
500	0.61	0.89	1.4	1.0	1.1
	(R8) $O + H_2 \rightarrow OH + H$[b]				
300	0.052	0.16	0.87	1.1	1.3
400	0.16	0.31	0.89	1.1	1.1
500	0.29	0.45	0.93	1.0	1.1

[a]GTST results, Ref. 83; accurate results, Ref. 84
[b]CVT, CVT/LAG, and accurate results, Refs. 34 and 85; CVT/MEPSAG, CVT/SCSAG, and CVT/LCG3 results, Ref. 85.

important, even at temperatures above room temperature. This point is illustrated by the fact that the CVT rate constant with no tunneling correction grossly underestimates the accurate rate constant values for all four reactions.

The reactions in Table III are arranged in order of increasing reaction–path curvature. Considering all four reactions as a group the LAG method provides the best overall agreement with the accurate quantal results. In three cases it provides a significant improvement over the SCSAG results at all temperatures considered, and in one case these methods are of comparable accuracy. Notice that the LAG results sometimes predict larger tunneling effects than the SCSAG results and sometimes predict smaller tunneling effects, because the approximations in the two methods are quite different. The LAG result for a given pair of tunneling path termini is always larger than the LCG3 one because the LCG3 tunneling path is a special (un–optimized) case of the LAG one. Thus when the methods differ appreciably the LAG result is always larger. When the results are similar, though, either one may be larger because of the semiclassical approach used in averaging over paths with various termini. In all cases shown, the $k^{CVT/LAG}(T)$ rate constants are in excellent agreement with the accurate quantal rate constants for 3–dimensional atom–diatom reactions.

TABLE IV. Ratios of 1–dimensional rate coefficients calculated with various tunneling approximations[a] to accurate quantal results.[b]

T,K	CVT	CVT/ MEPSAG	CVT/ SCSAG	CVT/ LCG	CVT/ LCG3	CVT/ LAG
	(R9) $^{37}Cl + H^{35}Cl \rightarrow {}^{37}ClH + {}^{35}Cl$					
200	0.13	0.15	0.15	0.61	0.61	0.55
300	0.33	0.35	0.35	0.81	0.82	0.76
600	0.82	0.83	0.83	1.2	1.2	1.2
1500	1.4	1.4	1.4	1.5	1.6	1.5
	(R10) $^{37}Cl + D^{35}Cl \rightarrow {}^{37}ClD + {}^{35}Cl$					
200	0.14	0.19	0.22	0.68	0.68	0.66
300	0.37	0.42	0.45	0.87	0.87	0.85
600	0.90	0.76	0.77	1.0	1.0	1.0
1500	1.4	1.3	1.3	1.4	1.4	1.4

[a]Previous GTST calculations on this system are reported in Refs. 32, 74, and 75. The present results (Ref. 86) all include anharmonicity by the WKB method.

[b]Calculated in Ref. 74 from data in Ref. 87.

There are no converged 3–D rate constants available for large–curvature systems, so we again return to the collinear world to compare to accurate quantal results; in particular, we consider the large curvature collinear reaction, $^{37}Cl + H^{35}Cl \rightarrow {}^{37}ClH + {}^{35}Cl$, and its isotopic analog, $^{37}Cl + D^{35}Cl \rightarrow {}^{37}ClD + {}^{35}Cl$ [46,74,85–90] The large ratios of the CVT/LAG rate coefficients to the CVT ones in Table IV indicate that tunneling is important; for example, LAG increases the rate for the H transfer case by about 30% for a temperature of 600 K and by a factor of ~4 at 200 K. The CVT/MEPSAG method provides little improvement over CVT, indicating that almost no tunneling occurs along the MEP path. The SCSAG method also fails badly in this case, but the LCG, LCG3, and LAG methods provide reasonable estimates of the tunneling contributions for both reactions, even though they do appear to consistently underestimate the tunneling effects at very low temperatures. (The LCG method is the original version of LCG3, and it gives very similar results.) Although accurate quantal results are not available for these reactions in the 3–dimensional case, it is interesting to compare to experiment, even though we are unable to separate the uncertainties in the potential surface from the uncertainties in the dynamical methods. From Table V, we see that tunneling is predicted to be important for both reactions in three dimensions; in reaction (R9) the calculated reaction rate increases by nearly an order of magnitude when tunneling is included at 368 K; in reaction (R10) this increase is smaller, at a factor of two and a half. In both cases the best calculated rate is in good agreement with experiment. The experimental results indicate that this system has only a moderate kinetic isotope effect, i.e., k(R9)/k(R10) = 5.0, yet from the theoretical results it is clear that tunneling contributions *are* important. In fact, the theoretical CVT kinetic isotope effect without tunneling contributions is less than 5%, indicating that there is almost no kinetic isotope effect at all in the absence of tunneling. Inclusion of tunneling in the theoretical calculations, however, brings the kinetic isotope effect much closer to the experimental value. Hence, moderate kinetic isotope effects do not necessarily mean that tunneling is unimportant for a reaction. This example provides a very significant caution about a common procedure for interpreting experimental data, by which tunneling effects are invoked only if the kinetic isotope effects are large. This example is particularly striking since the dominant tunneling paths are very

TABLE V. Comparison of 3–dimensional transition state theory rate constants (cm^3 $molecule^{-1}$ s^{-1}) and kinetic isotope effects with experiment at 368.2 K.[a]

	CVT	CVT/LCG	Expt.
k(R9)	3.8(–16)	3.3(–15)	5.1(–15)
k(R10)	3.7(–16)	9.8(–16)	1.0(–15)
k(R9)/k(R10)	1.0	3.3	5.0

[a]Theoretical results for the scaled surface of Garrett *et al.*, Ref. 46. Experimental results, Refs. 88–90.

far from the saddle point. Thus a conventional KIE interpretation based on saddle point force constants would be qualitatively misleading about what region of the energy surface is most critical in controlling the rate.

In some cases (e.g., [91]) neither the large–curvature nor the small–curvature limit is quantitatively reliable. In such cases the LAG method should be used for quantitative interpretation of kinetic isotope effects.

TABLE VI. Theoretical and experimental rate constants (cm^3 $molecule^{-1}$ s^{-1}) for the 3–dimensional reaction OH + $H_2 \rightarrow H_2O$ + H.

	CVT/SCSAG[a]		
T,K	Harmonic	Anharmonic	Experiment[b]
298	2.37(−14)	1.04(−14)	6.1±0.4(−15)
400	7.26(−14)	4.03(−14)	3.7±1.1(−14)
600	3.35(−13)	2.23(−13)	2.9±0.9(−13)
1000	1.91(−12)	1.42(−12)	2.4±0.7(−12)

[a]Ref. 9; the potential surface is described in Ref. 92.
[b]Ref. 93.

Finally we discuss two gas–phase reactions involving larger molecules. Table VI shows 3–dimensional CVT/SCSAG and experimental rate constants for the reaction OH + $H_2 \rightarrow H_2O$ + H [9,92,93]. The second column gives the $k^{CVT/SCSAG}(T)$ rate constant calculated as described above, with the independent–normal–mode harmonic approximation used to evaluate the partition functions for vibrational modes orthogonal to the reaction coordinate. The third column gives the $k^{CVT/SCSAG}(T)$ rate constant calculated with principal anharmonicity included in the independent–normal–mode representation of these vibrations. The agreement with experiment is good for both calculations, though it is generally better with the inclusion of anharmonicity. This agreement with experiment is quite impressive, since the potential energy surface used for these calculations is entirely *ab initio* [92,94,95], i.e., it was not calibrated to reproduce any experimental results. In general one would often be satisfied if good agreement could be obtained over a range of temperatures by adjusting only the barrier height.

We also consider the gas–phase reaction $CH_3 + H_2 \rightarrow CH_4 + H$ [48,96,97] for which the CVT/SCSAG results (only the lowest–frequency vibrational mode includes anharmonicity, the rest are treated harmonically) are tabulated and compared with an exemplary set of experimental results (two other sets are tabulated in Ref. 48) in Table VII. These calculated results, which are for the best semiempirical surface of Joseph *et al.* [48], are quite good; they differ from the experimental results by less than 20% for all temperatures at which the experimental results are available. We also compare calculated kinetic isotope effects with experiment. These results are tabulated in Table VIII and are also

TABLE VII. Calculated and experimental rate constants (cm^3 $molecule^{-1}$ s^{-1}) for the 3–dimensional reaction $CH_3 + H_2 \rightarrow CH_4 + H$.

T,K	CVT/SCSAG[a]	Experiment[b]
372	3.2(–18)	2.7(–18)
400	7.4(–18)	6.5(–18)
424	1.4(–17)	1.3(–17)
500	7.6(–17)	7.3(–17)
600	3.9(–16)	3.8(–16)
667	9.1(–16)	9.0(–16)

[a]Ref. 48, surface J3.
[b]Computed from reverse rate constants of Ref. 97 and JANAF equilibrium constants. See Ref. 48.

TABLE VIII. Kinetic isotope effects for the reactions $CH_3 + H_2 \rightarrow CH_4 + H$ (R12) and $CH_3 + D_2 \rightarrow CH_3D + D$ (R13).

	k(R12)/k(R13)	
T,K	CVT/SCSAG[a]	Experiment[b]
400	4.5	4.8±0.4
500	3.5	3.5±0.2
600	3.0	2.8±0.2
667	2.7	2.5±0.1

[a]Ref. 48; surface J3.
[b]Ref. 96.

quite good. Because the potential energy surface used to calculate the $CH_3 + H_2$ results is semiempirical, and the CVT/SCSAG method has already been shown to be reasonably reliable, the comparisons with experiment in Tables VII and VIII are really tests of the shape and calibration of the potential energy surface used. This then provides an example of how CVT/SCSAG rate constants and kinetic isotope effects are used to elucidate information regarding potential energy surfaces [48]. We note that the variational transition state for the $CH_3 + H_2$ reaction occurs slightly (~0.1 a_0) earlier than the saddle point, a result which agrees well with an earlier 3–body model [27] of this reaction based on a rotated-Morse-bond-energy-bond-order approximation to the energy surface. In both the full surface

and the 3–body model the variational displacement of the transition state is determined primarily by the stretching frequency of the mode that correlates to H–H stretching in reactants and to the new C–H stretch in products.

VTST may also be applied to unimolecular reactions in the gas phase [2,17,98] and the semiclassical tunneling approximations discussed here may be applied to conformational rearrangements such as switches of hydrogen bonds [99]. Generalizations of the ideas and methods presented above may also be used to treat reaction rates of vibrationally excited molecules [51] and the state–specific decay of metastable states [100].

6. Condensed–Phase Reactions

The quasi–thermodynamic formulation of transition state theory, especially the expression of the rate constant in terms of the free energy of activation, has been extremely useful in understanding differences in reaction rates between the gas phase and solution [19a]. Thus it is very important to understand the validity of transition state theory assumptions for solution reactions, and this question has recently received considerable attention [2,18,40]. Unlike gas–phase TST, which has received extensive testing against accurate classical and quantal dynamics, as discussed in Section 5, condensed–phase TST is much harder to test than gas–phase TST. In this section we discuss some of the new considerations which should be incorporated into generalized TST for reactions in solution. Generalized TST has also been applied to reactions on solid surfaces, and we shall discuss this as well. We consider both static effects, which are easily incorporated into the quasi-thermodynamic formalism developed for TST in the gas phase, and dynamic effects, which require careful interpretation. We note that generalized TST has a great advantage over many molecular dynamics techniques which are currently used for condensed–phase reactions because quantization effects and tunneling can be included by consistent procedures that have already been well tested for gas–phase processes.

Before proceeding to discuss the effect of solvent we note a formal difference between gas–phase and condensed–phase reactions. In condensed phases we do not have free translations and thus we cannot factor out free translational partition functions for each species, even though the partition functions for each species are still proportional to the volume of the system. Thus, by analogy to eq. (45) and eq. (35), eqs. (59a) and (59b) are replaced by

$$k^{GT}(T,s) = \sigma \frac{\tilde{k}T}{h} \frac{\Phi^{GT}(T,s)}{\Phi^{A}(T)\Phi^{B}(T)} e^{-\beta V_{MEP}(s)} \qquad \text{(bimolecular)} \tag{89a}$$

and

$$k^{GT}(T,s) = \sigma \frac{\tilde{k}T}{h} \frac{\Phi^{GT}(T,s)}{\Phi^{A}(T)} e^{-\beta V_{MEP}(s)} \qquad \text{(unimolecular),} \tag{89b}$$

respectively.

Because it is impossible to consider explicitly all of the solvent molecules in

a solution–phase reaction (or all of the atoms of the solid for a reaction on a crystalline surface) as part of the reacting system, all or most of the solvent molecules must be treated collectively as a "bath" — or ignored. A bath has both static and dynamical effects on a reacting system. Before considering these effects, we note that, if some solvent molecules (or solid–state atoms) play a significant role in the reaction coordinate, they *should* be treated explicitly as part of the primary reacting system rather than as part of the bath [18]. Thus, one should compromise between, on the one hand, minimizing computational effort by treating only a small number of solvent molecules (or solid–state atoms), if any, explicitly as part of the primary system and, on the other hand, accounting for important couplings between specific solvent molecules (or solid–state atoms) and the reaction coordinate. Once the primary system has been chosen, the effects of the bath on the rate constant for the primary system must be incorporated into the expression for this rate constant, eqs. (58) and (89). The simplest of these effects are static effects. In this first approximation, it is assumed that the bath solvent molecules (or solid–state atoms) adjust statistically to motions of the primary system, i.e., that the bath always remains in equilibrium with the primary system. The effect of the bath is then incorporated into the quasi–thermodynamic TST formalism [eq. (56) but without necessarily treating the left–hand side as classical] simply by considering its contribution to the free energy of the system (primary system plus bath) [1a,101]. Because the free energy of interaction of the bath and the system may vary greatly along the primary–system reaction coordinate, the free energy of activation, which directly determines the TST rate constant [see eq. (56)], may change drastically in the presence of the bath.

For many systems, however, it is questionable whether solvent (or surface) rearrangement is fast enough to allow solvent (or surface) equilibration at each step along the primary–system reaction coordinate. Such systems may exhibit dynamical, "nonequilibrium" solvation effects. As discussed in Section 2.4 equilibrium of phase space points originating in the reactants region is assured in classical mechanics if the reactants are in equilibrium and all molecules are treated explicitly; however, if we separate the system into a primary system and the rest, it may be a serious restriction to define the dividing surface entirely in terms of primary–system coordinates. In such a case the solvent is said to be "nonequilibrated" or to "participate in the reaction coordinate." The conceptually simplest way to include these effects is to include the solvent molecules or surface atoms showing the strongest interaction with the reacting solute (or adsorbate) in the primary system; this increases computational effort but avoids modifications to the TST formalism which, as described below, would otherwise be required to treat such nonequilibrium effects. This approach has been used successfully for treating the diffusion of hydrogen atoms on a metal surface [102–104]. Good convergence of reaction rates with respect to cluster size, i.e., with respect to the number of surface atoms included in the primary system, was achieved at and above room temperature, but convergence was harder to achieve below room temperature, because of the importance of tunneling. This indicates that tunneling is a more global, less localized phenomenon than classical barrier crossing. If dynamical solvent effects cannot be isolated to a treatably few solvent molecules or surface atoms, it is sometimes feasible to introduce a collective coordinate which can be included explicitly in the primary system. A good example of this technique is the introduction of a polarization vector when treating reactions in polar solvents [105–107].

In order to treat nonequilibrium solvation effects of bath molecules without

including them in the primary system, one may add a friction correction factor γ^{ζ} to the TST rate constant [18], e.g.,

$$k^{CVT/G,\zeta} = \gamma^{\zeta}{}_k k^{CVT/G}, \tag{90}$$

where the superscript on the correction factor indicates that it is determined by the degree of solvent friction on the primary system (ζ denotes a friction coefficient). In the case of solution reactions the friction correction factor may be approximated by a number of methods; among these are Kramers theory [108] and a generalized Langevin–equation approach [109,110]. Kramers theory is intended to account for a series of frequent, but weak, bath perturbations which interrupt motion along the reaction coordinate. In this theory the correction term is related to the ratio of the characteristic time scale for crossing the reaction coordinate barrier in the absence of friction to the characteristic time scale for relaxation of momentum along the reaction coordinate due to friction. The relaxation time due to friction may be estimated on the basis of the bulk viscosity of the solvent [18]. Work with the Langevin–equation approach, however, has indicated that the reaction rate is dependent upon the short–time solvent friction felt by the primary system [109,110], rather than on the bulk friction constant as used in Kramers theory; it is believed, therefore, that Kramers theory, with the relaxation time estimated from bulk viscosity usually overestimates the effect of friction on reaction rates [40]. An interesting perspective on the high–friction limit of Kramers theory is provided by a recent paper of Pollak [111]. Using a harmonic bath to model the generalized Langevin equation, Pollak showed that the frictional decrease of the rate calculated by TST for the primary system can also be calculated by doing TST (without friction) on the enlarged system consisting of the primary system plus the bath.

The dynamical friction effects that we have considered so far are based on the idea that the solvent molecules hinder the motion of the primary system along the reaction coordinate. This type of effect will predominate in the high–friction limit. There also may exist a regime where the time scale for barrier crossing is much faster than the time scale for solvent relaxation of reaction coordinate momentum, but still much slower than the time scale for energy redistribution in the reactant (see below). In this regime, the rate constant is expected to be independent of solvent friction. If there is very little coupling of the primary system to the solvent, however, the assumption that the reactants (or, for reversible reactions, the products, which are the reactants of the back reaction) are in local equilibrium may fail [108,112]. This failure results from the inability of collisions between primary system molecules and solvent molecules to exchange vibrational energy or to exchange vibrational with translational energy, and thus, the inability of these collisions to populate reactive regions of reactant phase space as rapidly as they are being depleted by reaction (or for reversible reactions, to depopulate highly excited nascent products before they react back), i.e., the time scale for energy redistribution in the reactants is slower than that for barrier crossing. This low–solvent–coupling regime is similar to the low–pressure limit for gas–phase reactions, as discussed in Section 2.4. Thus we expect three regimes for reactions in a bath. First, in the low–friction regime, the rate constant should increase with increasing friction as the reactant distribution of states approaches an equilibrium distribution. There may then be a regime where the reactant equilibrium assumption holds, but frictional effects on the reaction coordinate are

not yet important. In this regime the reaction rate constant will be independent of friction. Finally, as friction is increased still further, frictional slowing of reaction–coordinate motion becomes important, and the rate constant will decrease with increasing friction. This may be referred to as the "friction–controlled" regime. In both the first and third regimes, the uncorrected TST rate constant (even if this rate constant was calculated including static solvation effects) will overestimate the actual rate constant. In the middle, friction-independent regime, the uncorrected TST rate constant should be a good approximation to the true solution rate constant. Unfortunately, it is possible that, for many reactive systems, by the time the assumption of an equilibrium distribution of reactants is valid, frictional effects on the reaction coordinate will already be important, and the TST rate constant will overestimate the true rate constant in all cases if a correction term is not added [113,114].

Here we make two important notes. First, some studies of the importance of a friction correction term [113,114], as mentioned above, have been performed by including only the reacting solute in the primary system. It is possible that including just a few important solvent molecules in the primary system will yield a more realistic reaction coordinate, and, consequently, the TST or VTST dividing surface will be a better bottleneck, thus obviating the need for a friction correction term. Second, we note that recrossing of the transition state may cause errors in gas–phase TST rate constants, even when variational methods are used, of up to around a factor of two, especially for classical systems (see Section 5). One should be careful that these recrossing effects, which would be present even in the absence of solvent molecules, are not attributed to solvent friction when they occur for condensed–phase reactions. Detailed studies of a variety primary systems, both in the absence and in the presence of a solvent bath, could certainly help to clarify these issues. Both of these points raise uncertainties which cannot be resolved without further study.

Frictional effects occur in ultrahigh pressure gases as well as in solution [38]. In fact the binary–collision language of gas kinetics provides a simple way to think about the low–pressure and high–pressure fall–offs from the equilibrium plateau. At low pressures, when back reaction is neglected, the most energetic molecules, or the molecules with most energy in the most reactive modes, tend to react fastest, and energy–changing collisions are too infrequent to maintain thermal equilibrium concentrations of these states. For reversible reactions, collisions are also required to thermalize the products before they react back. At ultrahigh pressures, in contrast, collisions occur not only frequently enough to exchange energy on the kinetic time scale for reaction but also fast enough to interrupt the molecular motion along the reaction coordinate during a single reactive event.

Finally we mention a few recent applications of VTST and semiclassical tunneling concepts to organic reactions without invoking nonequilibrium, frictional, or solvation effects. In the language introduced at the beginning of this chapter these have all been based on the phenomenological approach rather than the absolute rate approach, and these concepts may be very useful for such reactions.

Houk and Rondan [115] and Doubleday *et al.* [116] have studied exothermic reactions with small or zero barriers. For such reactions the free energy of activation maximum may be controlled by the decrease in entropy of activation for generalized transition states located later along the reaction coordinate [117]. Since entropic effects become relatively more important compared to enthalpic

effects as the temperature is increased, this gives a handle for understanding temperture–dependent transition states and negative activation energies [115–117].

Kreevoy *et al.* [77] studied kinetic isotope effects for hydride transfer between carbons in nitrogen heterocycles, $R_1^+ + R_2H \rightarrow R_1H + R_2^+$. Quadratic free energy correlations indicated that the critical configurations for H^- transfer are geometrically more extended than those for D^-. This was interpreted in terms of large–curvature tunneling in which H^- tunnels at longer $R_1^+ - R_2^+$ distances than D^-.

7. Thermochemical Kinetics

In the quasi–thermodynamic formulation of transition state theory [eq.(56)], the transition state species is treated like a stable species, except that one degree of freedom, the unbound degree of freedom corresponding to the reaction coordinate, is removed. In conventional transition state theory, because the position of the dividing surface is determined entirely by the potential energy surface, i.e., the dividing surface is set at the saddle point, s = 0, the transition state species is independent of temperature. This is not true for the CVT transition state species, because the position of the dividing surface is re–optimized at each temperature. Thus, the conventional transition state can be related directly to a single molecular structure while the CVT transition state cannot. Using this relationship the quasi–thermodynamic quantities for the conventional transition state can be calculated directly from the temperature–independent structure and vibrational frequencies of the bound degrees of freedom of the conventional transition state. Furthermore, bond additivity and group additivity relationships can be used to approximate the enthalpy and the entropy [118]. In CVT, however, we must take account of the temperature dependence of the frequencies, bond strengths, and so forth.

The quasi–equilibrium constant, $K^{\ddagger}$, for the quasi–equilibrium between the reactants and the conventional transition state species is found from eq. (54) by setting s = 0, i.e.,

$$K^{\ddagger} = \sigma \frac{Q^{\ddagger}(T)}{\Phi^{R}(T)} e^{-V^{\ddagger}/\tilde{k}T} \quad \text{(bimolecular)}, \tag{91a}$$

$$K^{\ddagger} = \sigma \frac{Q^{\ddagger}(T)}{Q^{A}(T)} e^{-V^{\ddagger}/\tilde{k}T} \quad \text{(unimolecular)}, \tag{91b}$$

where we have replaced the classical partition functions with their quantum analogs, as discussed in Section 3, and we have defined $Q^{\ddagger}(T) = Q^{GT}(T,s=0)$ and $V^{\ddagger}(T) = V_{MEP}(s = 0)$. By analogy to eqs. (54)–(56), we can write the conventional TST rate constant in terms of a free–energy change between

reactants and the transition state species, $\Delta_{\ddagger}G^{0}_{T}$, as

$$k^{\ddagger}(T) = \frac{\tilde{k}T}{h} K^{0} e^{-\Delta_{\ddagger}G^{0}_{T}/RT}, \tag{92}$$

where $\Delta_{\ddagger}G^{0}_{T}$ is defined by the relationship

$$K^{\ddagger} = K^{0} e^{-\Delta_{\ddagger}G^{0}_{T}/RT} \tag{93}$$

The free energy of activation may be further partitioned in terms of the enthalpy and entropy of activation at temperature T, $\Delta_{\ddagger}H^{0}_{T}$ and $\Delta_{\ddagger}S^{0}_{T}$, respectively, as

$$\Delta_{\ddagger}G^{0}_{T} = \Delta_{\ddagger}H^{0}_{T} - T\,\Delta_{\ddagger}S^{0}_{T}. \tag{94}$$

From eqs. (92) and (94), one could evaluate the conventional TST rate constant by evaluating $\Delta_{\ddagger}H^{0}_{T}$ and $\Delta_{\ddagger}S^{0}_{T}$, i.e., by evaluating the quasi–thermodynamic properties of the conventional transition state.

However, in systems where the conventional transition state does not provide a good bottleneck or where tunneling contributions are important, $k^{\ddagger}$ will not be a very good approximation to the actual rate [14–18]. A much better approximation for such systems would be $k^{CVT/G}$ defined in eq. (58b), which includes a ground–state transmission coefficient, $\kappa^{CVT/G}(T)$, as discussed in Section 4. For simplicity, we shall consider only the LAG approximation for the transmission coefficient in this section. Further, let us define the more concise notation, $\kappa_{tun}(T)$, where, for the methods suggested above,

$$\kappa_{tun}(T) \equiv \kappa^{CVT/LAG}(T). \tag{95}$$

If we define $\kappa_{var}(T)$, the contribution to the rate due to the optimization of the dividing surface position as a function of temperature, as

$$\kappa_{var}(T) = k^{CVT}(T)/k^{\ddagger}(T), \tag{96}$$

we can factor the rate constant, eq. (58b), as

$$k^{CVT/LAG}(T) = \kappa_{tun}(T)\kappa_{var}(T)k^{\ddagger}(T). \tag{97}$$

With this factorization, it is clear that one contribution, $k^{\ddagger}(T)$, to the rate constant, $k^{CVT/LAG}(T)$, is determined by a "substance" — the conventional transition state species — and its properties. This type of contribution is called a

substantial contribution [119]. The other two terms κ_{tun} and κ_{var}, do not depend only upon a single transition state species, but rather require characterization of the system along part or all of the reaction path as a function of temperature. Thus, this type of contribution is called a nonsubstantial contribution [119].

For the nonsubstantial contributions it is useful to introduce a factorization analogous to that used for the substantial contributions [eqs. (93) and (94)]. This factorization is [119]

$$\kappa_x(T) = \exp(\Delta_{n_x}S^0_T/R)\exp(-\Delta_{n_x}H^0_T/RT), \tag{98}$$

where $\Delta_{n_x}S^0_T$ and $\Delta_{n_x}H^0_T$ are nonsubstantial activation parameters which parameterize contributions for temperature–independent and temperture–dependent factors in $\kappa_x(T)$. These nonsubstantial parameters are obtained from the relations

$$\Delta_{n_x}S^0_T = RT\,\frac{d\ \ell n\ \kappa_x}{dT} + R\ \ell n\ \kappa_x \tag{99}$$

$$\Delta_{n_x}H^0_T = RT^2\,\frac{d\ \ell n\ \kappa_x}{dT}, \tag{100}$$

which are analogous to the Gibbs–Helmholtz relations between the entropy and enthalpy and the equilibrium constant for a given system. Both $\kappa_{tun}(T)$ and $\kappa_{var}(T)$ are factorized as in eq. (98) suggesting

$$\Delta_aH^0_T = \Delta_{tun}H^0_T + \Delta_{var}H^0_T + \Delta_{\ddagger}H^0_T \tag{101}$$

and

$$\Delta_aS^0_T = \Delta_{tun}S^0_T + \Delta_{var}S^0_T + \Delta_{\ddagger}S^0_T, \tag{102}$$

such that eq. (97) is equivalent to

$$k^{CVT/LAG}(T) = \frac{\tilde{k}T}{h}\,K^0\,e^{\Delta_aS^0_T/R}\,e^{-\Delta_aH^0_T/RT}, \tag{103}$$

which is reminiscent of eq. (56) if we define

$$\Delta_aG^0_T = \Delta_aH^0_T - T\Delta_aS^0_T. \tag{104}$$

Equations (101)–(103) clearly illustrate that to provide a good estimate of the rate constant for systems where tunneling or variational effects are important, the nonsubstantial contributions must be included in the entropy and enthalpy of activation [119].

The specific factorization of the rate constant, as given by eq. (97), which yields the separation of enthalpic and entropic terms as given by eq. (101) and eq.

(102), is particularly useful if one has information about the potential energy surface, and thus about the properties of the saddle point species, since this information allows for the calculation of $\Delta_{\ddagger}S^{0}_{T}$ and $\Delta_{\ddagger}H^{0}_{T}$. Another possible factorization, which could be more useful for the interpretation of experimental data, is one which maximizes the substantial contributions to entropy and enthalpy, while minimizing the nonsubstantial contributions [119]. One such factorization is based on a single temperture-independent transition state which is set at the maximum, denoted by $s = s^{AG}_{*}$, of the adiabatic ground–state potential curve, $V^{G}_{a}(s)$ [eq. (72)], instead of at the saddle point. Alternatively it could be set at the location of the maximum free energy of activation for the center of the temperature interval of interest; the maximum of $V^{G}_{a}(s)$, in contrast, would be the variational, or CVT, transition state location for a temperature of 0 K. Thus, we can define a correction factor for the temperature dependence of the transition state location $\kappa_{therm}(T)$ as

$$\kappa_{therm}(T) = k^{CVT}(T)/k^{GT}(T,s^{AG}_{*}), \tag{105}$$

and the factorization, analogous to eq. (97), becomes

$$k^{CVT/LAG}(T) = \kappa_{tun}(T)\kappa_{therm}(T)k^{GT}(T,s^{AG}_{*}), \tag{106}$$

where $k^{GT}(T,s^{AG}_{*})$ gives rise to the substantial part of the enthalpy and entropy. With this factorization, we have for the nonsubstantial contributions to $\Delta_{a}H^{0}_{T}$ and $\Delta_{a}S^{0}_{T}$,

$$\Delta_{n}H^{0}_{T} = \Delta_{tun}H^{0}_{T} + \Delta_{therm}H^{0}_{T} \tag{107}$$

$$\Delta_{n}S^{0}_{T} = \Delta_{tun}S^{0}_{T} + \Delta_{therm}S^{0}_{T}. \tag{108}$$

For several hydrogen–atom transfer reactions with barriers of about 10 kcal/mol, it has been found [119] that $\Delta_{therm}H^{0}_{T}$ and $\Delta_{therm}S^{0}_{T}$ are small, especially at low temperatures where $\Delta_{tun}H^{0}_{T}$ and $\Delta_{tun}S^{0}_{T}$ are very significant. Table IX gives an example [119] for the O + H_2 reaction. We see, e.g., that the temperature dependences of the total enthalpy and entropy of activation are both opposite in direction to their substantial parts. As a result of the temperature dependences of both activation parameters the phenomenological Arrhenius activation energy decreases from 14 kcal/mol at T = 1400–1900 K to 8 kcal/mol at 318–471 K [120]. The latter value is considerably smaller than the saddle point height, which is 12½ kcal/mol.

TABLE IX. Activation parameters for $O(^3P) + H_2 \rightarrow OH + H$.[a]

		T=200 K	T=1500K
ΔH (kcal/mol)	substantial	9.7	7.8
	therm	0.0	–0.1
	tun	–5.7	–0.3
total enthalpy of activation		4.0	7.4
ΔS (e.u.)	substantial	–19.6	–23.6
	therm	0.0	–0.1
	tun	–14.8	–0.1
total entropy of activation		–34.4	–23.8

[a]standard state = 1 atm.

8. Concluding Remarks

We have seen that transition state theory methods yield consistently good results when applied to gas–phase reactions. Variational methods and quantum corrections require more computational effort and more potential energy information than conventional transition state theory, but they yield much better results. We now have carried out and interpreted enough calculations to allow us to make informed decisions about which methods are required for various systems, based on a knowledge of barrier heights, vibrational frequencies, particle masses, and/or reaction–path curvature, as well as on which temperatures are of interest. Applications to larger and more complex systems are limited to a large degree by the availability of potential energy information, not by the state of the dynamical theories. The use of transition state theory to calculate reaction rates in condensed phases and at heterogeneous interfaces is just beginning, as is the understanding of extensions which may be required or useful for describing these systems, yet we are already witnessing some successful applications to these types of systems. Finally, we have tried to stress that more complicated aspects of reactions, which may be elucidated by examining variational and semiclassical tunneling corrections to conventional transition state theory, often play a large part in determining reaction rates, and must be considered when interpreting experimental results; otherwise their effects may be incorrectly attributed in the phenomenological analyses.

9. Acknowledgments

The authors are grateful to Bruce C. Garrett for long–standing and continuing collaboration on the subject of these review lectures and to the organizers of the NATO–ASI Workshop for making it possible for us to participate. This work was supported in part by the U.S. Department of Energy, Office of Basic Energy Sciences.

References

1. S. Glasstone, K. Laidler, and H. Eyring, *The Theory of Rate Processes* (McGraw–Hill, New York, 1941), pp. 10–16, (a) pp. 401–403.

2. D. G. Truhlar, W. L. Hase, and J. T. Hynes, *J. Phys. Chem.* **87**, 2664, 5523(E) (1983).

3. J. W. Moore and R. G. Pearson, *Kinetics and Mechanism*, 3rd ed. (John Wiley & Sons, New York, 1981), p. 163.

4. E. Wigner, *J. Chem. Phys.* **5**, 720 (1937).

5. J. C. Keck, *Adv. Chem. Phys.* **13**, 85 (1967).

6. B. H. Mahan, *J. Chem. Educ.* **51**, 709 (1974).

7. W. H. Miller, *J. Chem. Phys.* **61**, 1823 (1974).

8. B. C. Garrett and D. G. Truhlar, *J. Phys. Chem.* **83**, 1052 (1979), **87**, 4553(E) (1983).

9. A. D. Isaacson and D. G. Truhlar, *J. Chem. Phys.* **76**, 1380 (1982).

10. E. B. Wilson, Jr., J. C. Decius, and P. C. Cross, *Molecular Vibrations* (Dover, New York, 1980), p. 14.

11. G. Arfken, *Mathematical Methods for Physicists* (Academic Press, New York, 1970), p. 34, (a) p. 32, (b) p. 48.

12. H. Goldstein, *Classical Mechanics*, 2nd ed. (Addison–Wesley Publishing Company, Reading, MA, 1980), p. 556, (a) p. 426.

13. D. A. McQuarrie, *Statistical Mechanics* (Harper and Row, New York, 1976), §7–1.

14. J. B. Anderson, *J. Chem. Phys.* **58**, 4684 (1973).

15. D. G. Truhlar and B. C. Garrett, *Acc. Chem. Res.* **13**, 440 (1980).

16. E. Wigner, *Trans. Faraday Soc.* **34**, 29 (1938).

17. D. G. Truhlar, A. D. Isaacson, and B. C. Garrett, in *Theory of Chemical Reaction Dynamics*, edited by M. Baer (CRC Press, Boca Raton, FL, 1985), Vol. 4, p. 1.

18. M. M. Kreevoy and D. G. Truhlar, in *Investigation of Rates and Mechanisms of Reactions* (*Techniques of Chemistry*, edited by A. Weissberger, 4th ed., Vol. 6), edited by C. F. Bernasconi (John Wiley & Sons, New York, 1986), Part 1, p. 13.

19. R. E. Weston, Jr. and H. A. Schwarz, *Chemical Kinetics* (Prentice–Hall, Inc. Engelwood Cliffs, NJ, 1972), p. 100, (a) § 6.7–6.8.

20. I. Shavitt, University of Wisconsin Theoretical Chemistry Laboratory Technical Report No. WIS–AEC–23, Madison, WI, 1959.

21. R. A. Marcus, *J. Chem. Phys.* **49**, 2610 (1968).

22. D. G. Truhlar and A. Kuppermann, *J. Amer. Chem. Soc.* **93**, 1840 (1971).

23. K. Fukui, in *The World of Quantum Chemistry*, edited by R. Daudel and B. Pullman (D. Reidel, Dordrecht, Holland, 1974), p. 113.

24. H. F. Schaefer, III, *Chem. Brit.* **11**, 227 (1975).

25. D. G. Truhlar, F. B. Brown, R. Steckler, and A. D. Isaacson, in *The Theory of Chemical Reaction Dynamics*, edited by D. C. Clary (D. Reidel, Dordrecht, Holland, 1986), p. 285.

26. B. C. Garrett, M. J. Redmon, R. Steckler, D. G. Truhlar, K. K. Baldridge, D. Bartol, M. W. Schmidt, and M. S. Gordon, *J. Phys. Chem* **92**, 1476 (1988).

27. B. C. Garrett and D. G. Truhlar. *J. Amer. Chem. Soc.* **101**, 4534 (1979).

28. B. C. Garrett and D. G. Truhlar, *J. Amer. Chem. Soc.* **102**, 2559 (1980).

29. D. G. Truhlar, A. D. Isaacson, R. T. Skodje, and B. C. Garrett, *J. Phys. Chem.* **86**, 2252 (1982).

30. B. C. Garrett and D. G. Truhlar, *J. Phys. Chem.* **83**, 1079 (1979), **87**, 4553(E) (1983).

31. B. C. Garrett, D. G. Truhlar, R. S. Grev, and A. W. Magnuson, *J. Phys. Chem.* **84**, 1730 (1980), **87**, 4554(E) (1983).

32. B. C. Garrett and D. G. Truhlar, *J. Chem. Phys.* **81**, 309 (1984).

33. D. G. Truhlar and B. C. Garrett, *Annu. Rev. Phys. Chem.* **35**, 159 (1984).

34. B. C. Garrett, D. G. Truhlar, and G. C. Schatz, *J. Amer. Chem. Soc.* **108**, 2876 (1986).

35. D. G. Truhlar and B. C. Garrett, *J. Chim. Phys.* **84**, 365 (1987).

36. P. J. Robinson and K. A. Holbrook, *Unimolecular Reactions* (John Wiley & Sons, New York, 1972).

37. W. Forst, *Theory of Unimolecular Reactions* (Academic Press, New York, 1973).

38. J. Troe, in *Kinetics of Gas Reactions* (*Physical Chemistry: An Advanced Tretise*, edited by H. Eyring, D. Henderson, and W. Jost, Vol. VI B), edited by W. Jost (Academic Press, New York, 1975), p. 835.

39. C. Lim and D. G. Truhlar, *J. Phys. Chem.* **90**, 2616 (1986).

40. J. T. Hynes, in *Theory of Chemical Reaction Dynamics*, edited by M. Baer (CRC Press, Boca Raton, FL, 1985), Vol. 4, p. 171.

41. I. Mayer, *J. Chem. Phys.* **60**, 2564 (1974).

42. R. C. Tolman, *The Principles of Statistical Mechanics* (Oxford University Press, New York, 1938), §19.

43. P. Pechukas, in *Dynamics of Molecular Collisions, Part B*, edited by W. H. Miller (Plenum Press, New York, 1976), p. 239.

44. E. E. Nikitin, *Theory of Elementary Atomic and Molecular Processes in Gases* (Clarendon Press, Oxford, 1974), chap. 1.

45. I. W. M. Smith, *Kinetics and Dynamics of Elementary Gas Reactions* (Butterworths, London, 1980), §4.2.3.

46. B. C. Garrett, D. G. Truhlar, A. F. Wagner, and T. H. Dunning, Jr., *J. Chem. Phys.* **78**, 4400 (1983).

47. P. Valtzanos and K. Ruedenberg, *Theoret. Chim. Acta* **69**, 281 (1986).

48. T. Joseph, R. Steckler, and D. G. Truhlar, *J. Chem. Phys.* **87**, 7036 (1987).

49. D. G. Truhlar, *J. Chem. Phys.* **56**, 3189 (1972), **61**, 440(E) (1974).

50. A. F. Wagner, J. M. Bowman, and L. B. Harding, *J. Chem. Phys.* **82**, 1866 (1985).

51. B. C. Garrett and D. G. Truhlar, *Int. J. Quantum Chem.* **29**, 1463 (1986).

52. J. O. Hirschfelder and E. Wigner, *J. Chem. Phys.* **7**, 616 (1939).

53. M. A. Eliason and J. O. Hirschfelder, *J. Chem. Phys.* **30**, 1426 (1959).

54. L. Hofacker, *Z. Naturforsch.* **18a**, 607 (1963).

55. R. A. Marcus, *J. Chem. Phys.* **43**, 1598 (1965).

56. D. G. Truhlar, *J. Chem. Phys.* **53**, 2041 (1970).

57. W. H. Miller, *J. Chem. Phys.* **65**, 2216 (1975).

58. B. C. Garrett and D. G. Truhlar, *J. Chem. Phys.* **76**, 1853 (1982).

59. R. L. Liboff, *Introductory Quantum Mechanics* (Holden–Day, Inc. San Francisco, 1980), §7.7.

60. A. S. Davydov, *Quantum Mechanics*, translated and edited by D. ter Haar (Addison–Wesley Publishing Company, Inc., Reading, MA, 1968), §26.

61. E. Merzbacher, *Quantum Mechanics* (John Wiley & Sons, New York, 1970), chap. 7.

62. E. C. Kemble, *The Fundamental Principles of Quantum Mechanics with Elementary Applications* (Dover, New York, 1937).

63. W. H. Miller, *Faraday Discuss. Chem. Soc.* **62**, 40 (1977).

64. B. C. Garrett and D. G. Truhlar, *J. Phys. Chem.* **83**, 2921 (1979).

65. R. D. Levine and R. B. Bernstein, *Molecular Reaction Dynamics and Chemical Reactivity* (Oxford University Press, New York, 1987), p. 165.

66. M. J. Stern, A. Persky, and F. S. Klein, *J. Chem. Phys.* **58**, 5697 (1973).

67. R. A. Marcus, *J. Chem. Phys.* **45**, 4493 (1966).

68. A. Kuppermann, J. T. Adams, and D. G. Truhlar, Abstr. Pap. Int. Conf. Phys. Electron. At. Collisions, 8th, 149 (1973).

69. A. Kuppermann, in *Theory of Scattering: Papers in Honor of Henry Eyring* (*Theoretical Chemistry*, Vol. 6A, edited by D. Henderson, Academic, New York, 1981), p. 80.

70. R. A. Marcus and M. E. Coltrin, *J. Chem. Phys.* **67**, 2609 (1977).

71. R. T. Skodje, D. G. Truhlar, and B. C. Garrett, *J. Phys. Chem.* **85**, 3019 (1981).

72. W. H. Miller, N. C. Handy, and J. E. Adams, *J. Chem. Phys.* **72**, 99 (1980).

73. V. K. Babamov and R. A. Marcus, *J. Chem. Phys.* **74**, 1790 (1981).

74. D. K. Bondi, J. N. L. Connor, B. C. Garrett, and D. G. Truhlar, *J. Chem. Phys.* **78**, 5981 (1983).

75. B. C. Garrett and D. G. Truhlar, *J. Chem. Phys.* **79**, 4931 (1983).

76. B. C. Garrett, N. Abusalbi, D. J. Kouri, and D. G. Truhlar, *J. Chem. Phys.* **83**, 2252 (1985).

77. M. M. Kreevoy, D. Ostović, D. G. Truhlar, and B. C. Garrett, *J. Phys. Chem.* **90**, 3766 (1986).

78. R. Steckler, K. J. Dykema, F. B. Brown, G. C. Hancock, and D. G. Truhlar, *J. Chem. Phys.* **87**, 7024 (1987).

79. D. G. Truhlar and B. C. Garrett, *J. Phys. Chem.* **84**, 805 (1980).

80. J. C. Gray, D. G. Truhlar, L. Clemens, J. W. Duff, F. M. Chapman, Jr., G. O. Morrell, and E. F. Hayes, *J. Chem. Phys.* **69**, 240 (1978).

81. J. A. Kaye and A. Kuppermann, *Chem. Phys. Lett.* **77**, 573 (1981).

82. D. G. Truhlar, B. C. Garrett, P. G. Hipes, and A. Kuppermann, *J. Chem. Phys.* **81**, 3542 (1984).

83. G. C. Lynch, D. G. Truhlar, and B. C. Garrett, manuscript in preparation.

84. D. C. Clary, *J. Chem. Phys.* **83**, 1685 (1985).

85. B. C. Garrett and D. G. Truhlar, unpublished.

86. S. C. Tucker, G. C. Lynch, B. C. Garrett, and D. G. Truhlar, unpublished.

87. D. K. Bondi, J. N. L. Connor, J. Manz, and J. Römelt, *J. Mol. Phys.* **50**, 467 (1983).

88. F. S. Klein, A. Persky, and R. E. Weston, Jr., *J. Chem. Phys.* **41**, 1799 (1964).

89. A. Persky and F. S. Klein, *J. Chem. Phys.* **44**, 3617 (1966).

90. J. H. Lee, J. V. Michael, W. A. Payne, L. J. Stief, and D. A. Whytock, *J. Chem. Soc. Faraday Trans. I* **73**, 1530 (1977).

91. S. C. Tucker, D. G. Truhlar, B. C. Garrett, and A. D. Isaacson, *J. Chem. Phys.* **82**, 4102 (1985).

92. G. C. Schatz and H. Elgersma, *Chem. Phys. Lett.* **73**, 21 (1980).

93. A. R. Ravishankara, J. M. Nicovich, R. L. Thompson, and F. P. Tully, *J. Phys. Chem.* **85**, 2498 (1981).

94. S. P. Walch and T. H. Dunning, Jr., *J. Chem. Phys.* **72**, 1303 (1980).

95. T. H. Dunning, Jr., S. P. Walch, and A. F. Wagner, in *Potential Energy Surfaces and Dynamics Calculations*, edited by D. G. Truhlar (Plenum, New York, 1981), p. 329.

96. J. S. Shapiro and R. E. Weston, Jr., *J. Phys. Chem.* **76**, 1669 (1972).

97. R. Shaw, *J. Phys. Chem. Ref. Data* **7**, 1179 (1978).

98. W. L. Hase, *Acc. Chem. Res.* **16**, 258 (1983).

99. G. C. Hancock, P. Rejto, R. Steckler, F. B. Brown, D. W. Schwenke, and D. G. Truhlar, *J. Chem. Phys.* **85**, 4997 (1986).

100. R. T. Skodje, D. W. Schwenke, D. G. Truhlar, and B. C. Garrett, *J. Phys. Chem.* **88**, 628 (1984).

101. I. D. Clark and R. P. Wayne, in *The Theory of Kinetics* (*Comprehensive Chemical Kinetics*, Vol. 2), edited by C. H. Bamford and C. F. H. Tipper (Elsevier, Amsterdam, 1969), p. 302.

102. J. G. Lauderdale and D. G. Truhlar, *J. Chem. Phys.* **84**, 1843 (1986).

103. T. N. Truong and D. G. Truhlar, *J. Phys. Chem.* **91**, 6229 (1987).

104. T. N. Truong and D. G. Truhlar, *J. Chem Phys.* **88**, 6611 (1988).

105. G. van der Zwan and J. T. Hynes, *J. Chem. Phys.* **78**, 4714 (1983).

106. G. van der Zwan and J. T. Hynes, *Chem. Phys.* **90**, 21 (1984).

107. B. J. Gertner, J. P. Bergsma, K. R. Wilson, S. Lee, and J. T. Hynes, *J. Chem. Phys.* **86**, 1377 (1987).

108. H. A. Kramers, *Physica* (The Hague) **7**, 284 (1940).

109. R. F. Grote and J. T. Hynes, *J. Chem. Phys.* **73**, 2715 (1980).

110. S. A. Adelman and C. L. Brooks, *J. Phys. Chem.* **86**, 1511 (1982).

111. E. Pollak, *J. Chem. Phys.* **85**, 865 (1986).

112. J. M. Montgomery, Jr., D. Chandler, and B. J. Berne, *J. Chem. Phys.* **70**, 4056 (1979).

113. J. L. Skinner and P. G. Wolynes, *J. Chem. Phys.* **72**, 4913 (1980).

114. G. T. Evans, *J. Chem. Phys.* **78**, 4963 (1983).

115. K. N. Houk and N. G. Rondan, *J. Amer. Chem. Soc.* **106**, 4293 (1984).

116. C. Doubleday, J. McIver, M. Page, and T. Zielinski, *J. Amer. Chem. Soc.* **107**, 5800 (1985).

117. S. N. Rai and D. G. Truhlar, *J. Chem. Phys.* **79**, 6046 (1983).

118. S. W. Benson, *Thermochemical Kinetics*, 2nd ed. (John Wiley & Sons, New York, 1976).

119. D. G. Truhlar and B. C. Garrett, *J. Amer. Chem. Soc.*, in press.

120. B. C. Garrett, D. G. Truhlar, J. M. Bowman, A. F. Wagner, D. Robie, S. Arepalli, N. Presser, and R. J. Gordon, *J. Amer. Chem. Soc.* **108**, 3515 (1986).